# DESIGN OF A PIEZOELECTRICALLY ACTUATED MICROVALVE FOR FLOW CONTROL IN FUEL CELLS

by

Ahmet Fatih Ayhan

BS Mechanical Engineering, Middle East Technical University, 2000

Submitted to the Graduate Faculty of

School of Engineering in partial fulfillment

of the requirements for the degree of

Master of Science in Mechanical Engineering

University of Pittsburgh

***2002***

UNIVERSITY OF PITTSBURGH

SCHOOL OF ENGINEERING

This thesis was presented

By

Ahmet Fatih Ayhan

It was defended on

04/10/2002

and approved by

Thesis Advisor: Jeffrey S. Vipperman, Ph. D.

DESIGN OF A PIEZOELECTRICALLY ACTUATED MICROVALVE FOR FLOW CONTROL IN FUEL CELLS

Ahmet Fatih Ayhan, MS

University of Pittsburgh, 2002

This thesis presents a novel piezoelectrically actuated microvalve for flow control in fuel cells. A fuel cell is an electrochemical device, which directly converts chemical energy stored in a fuel (e.g. hydrogen) and an oxidizer (e.g. oxygen) directly into electrical energy. Poor flow distributions within the cell have been attributed to degraded performance and even damage.

In this study, it is proposed to embed microvalves directly into the fuel cells to manage the gas flows and improve efficiency, performance, and reliability. The microvalve has four parts. The actuator is a piezoelectric trimorph which has two piezoelectric layers and one brass layer sandwiched between them and has dimensions of $20000 \times 4000 \times 290$ microns. It also has a valve gate placed on the tip. For a 5-volt input, a deflection of 32 microns can be achieved in the trimorph tip, which is what modulates the flow through the valve.

The valve design and analysis are complete. Maximum stress on the bender reaches up to 60 MPa when the fluidic and thermal forces are at their maximum. This maximum stress is below the tensile dynamic strength values of piezoelectric and brass layers used. A minimum factor of safety of 1.5 is obtained at 20°C. At the operating temperature, which is about 100°C

the factor of safety is around 13. The drag and pressure forces are found to reduce the free deflection by only 0.2 microns whereas the thermal expansion forces increases the deflection almost by the same amount. Finally detailed fabrication plan and drawings were completed.

## ACKNOWLEDGEMENTS

*"This thesis is dedicated to my sister Ayca Ayhan…"*

Firstly, I would like to thank my advisor Dr. Jeffrey S. Vipperman for his support, guidance and enthusiasm throughout this research. I would also like to acknowledge the support that I received from Dr. Qing-Ming Wang, Dr. William W. Clark and Dr. Dipo Onipede.

I would like to thank all members of the Sound Systems and Structures Laboratory that I worked with during the course of this research. In particular, I would like to thank Deyu Li and Ilya Avdeev for their help.

Thanks go to my parents, my sister, friends, Baris Taskin and Ozlem Durmaz whose support and help kept me motivated and concentrated on my work.

The author also gratefully acknowledges the support of the National Energy Technology Laboratory (NETL).

Thank you.

## TABLE OF CONTENTS

## LIST OF TABLES

## LIST OF FIGURES

# 1.0 INTRODUCTION

Energy has always been one of the main concerns of human being. Its importance and the need for energy have been increasing with increasing world population and growing industry.

In 1900's, with industry revolution, energy shortage has become a big problem. To overcome this problem the number of power plants increased dramatically to produce more energy, and this lead to new problems. Coal power plants, nuclear plants, combustion engines and hydroelectric power plants have always come with the problems of air pollution, noise, lack of efficiency, high cost and fatal danger. Then, people started to think about new power supply systems with less noise, emissions and danger yet with a high efficiency.

Fuel cells seem to be the best solution ever for the clean, efficient and non-hazardous energy. Ludwig Mond and Carl Langer produced the first fuel cell in 1889. In the next century, there have been great efforts to improve fuel cell systems. Today, high efficiency fuel cells are available for many applications. But these energy conversion devices still have problems and they still need to be improved.

Fuel cells are used as stacks for practical applications since the output of a single cell does not produce enough voltage. One notable problem associated with fuel cell stacks is the poor distribution of the reactants, which causes a decrease in efficiency and sometimes a damage to the system itself.

In this thesis, a new piezoelectrically actuated microvalve is proposed to solve this problem. In the first part of the thesis, fuel cells are introduced. Basic fuel cell structure, operating principles, performance characteristics and applications are explained in the first part. The characteristics of PEM type fuel cells, which the microvalve is designed for, are explained in another section. After reviewing PEM fuel cell characteristics, the problem statement is made. In the second part of the thesis, microvalves and MEMS technology are reviewed. General characteristics of microvalves, their applications, classifications and actuation methods are explained. A brief comparison of actuation methods is made and the reasons for the use of piezoelectric actuation are explained. The next two parts give the details of design, analysis and fabrication including finite element analysis results, fluidic and thermal analysis and step by step fabrication processes. The obtained results are compared and conclusions are derived. Finally some future work that would increase the valve performance is proposed.

## 2.0 FUEL CELLS

Fuel cell is an electrochemical device, which directly converts chemical energy into electrical energy. Although fuel cells have components similar to those of typical batteries, fuel cells are different than batteries. They are not energy storage devices; they can supply energy as long as the fuel and the oxidant are supplied.

William Robert Grove (1811-1896) is considered as the father of fuel cell technology. He produced hydrogen/oxygen fuel cells connected to electrolysis for decomposition of water to hydrogen and oxygen. He also made fuel cells with ethylene and carbon monoxide. Ludwig Mond and Carl Langer produced a gas-powered battery and called their system a fuel cell in 1889. In 1855, Antonio Becquerel made a new type of battery and used a carbon rod. Dr. William W. Jacques further explored the carbon approach in 1896. His fuel cells had a carbon rod central anode in the electrolyte of molten potassium hydroxide. He made a fuel cell system of 100 cylindrical cells, which produced as much as 1500 watts. Francis Bacon worked on fuel cells to produce alkaline systems that did not use noble metal catalysts in 1930's. He developed and built a 6 kW alkaline hydrogen/oxygen system in 1959. In the same year, Dr. Harry Ihrig introduced the first fuel cell tractor. Then a one-man submarine powered by a hydrazine and compressed oxygen fuel cell was produced. Fuel cells are used to supply power and drinking water in space. First stationary fuel cell power plant, PC-25, was developed by International Fuel Cell Corporation.

Fuel cell application areas have been growing constantly for years. Besides stationary power plants, they are also used for motive power for vehicles, airplane propulsion, cell phones and army systems. Army systems include battery charging devices, mobile power systems, generators, power sensor suites, coast guard buoys, power UAV/robots, PM physical security, PM soldier, landwarrior, power mini/TOC, SOF and situational awareness. Fuel cells are also used to replace diesel and turbine generators in navy ships.

## 2.1 Fuel Cell Components

Basically, a fuel cell consists of two electrodes sandwiched around an electrolyte. One electrode is negative and it is called the anode. The other electrode is positive and it is called the cathode. There are catalysts on either side of the electrolyte to increase the reaction rate at the electrodes. Electrodes and electrolyte have different functions for fuel cell operation.

A schematic of a fuel cell is given in Figure 1. Two electrodes at either side colored differently. $H^+$ and $e^-$ flow directions are from anode (-) to cathode (+) in this example.

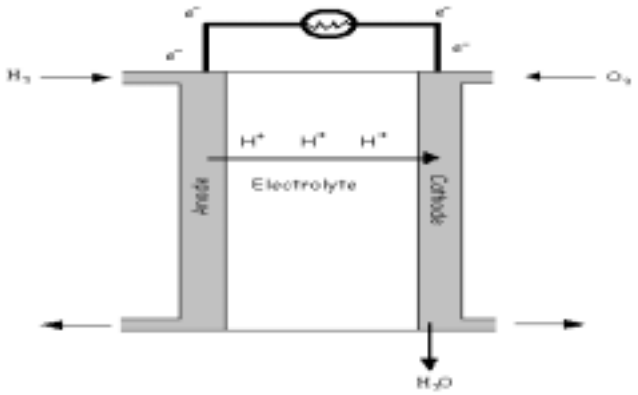


Figure 1 Schematic of a Fuel Cell

The electrolyte in fuel cells transports dissolved reactants to the electrode and conducts ionic charge between the electrodes i.e., completes the cell electric circuit. It can be either positive or negative. This affects the site of water production and removal. If the electrolyte is negative, the water production will be at the anode side. If the electrolyte is positive the water production will be at the cathode side. The electrolyte also provides a physical barrier to prevent the fuel and the oxidant gas streams from directly mixing. Different electrolytes are used for different applications and operating conditions.

Two electrodes, the cathode and the anode, have important functions. They conduct ions and provide a surface site where gas/liquid ionization or de-ionization reactions take place. They also provide a physical barrier that separates the bulk gas phase and the electrolyte. In order to increase the reaction rates, the electrode material should be catalytic, conductive and porous.

## 2.2 Fuel Cell Operation

Fuel cells produce electricity through an electrochemical reaction between the fuel and the oxidant. Gaseous hydrogen has become the fuel of choice because of its high reactivity when suitable catalysts are used and its high energy density when stored cryogenically. Hydrogen can be obtained from any hydrocarbon fuel, from natural gas to methanol, and even coal or gasoline with a fuel reformer. Pure hydrogen can be used without a fuel reformer. The most commonly used oxidant is gaseous oxygen since it is readily and economically available from air and easily stored in a closed environment.

Hydrogen fuel is fed into the anode of the fuel cell. Oxygen, or air, is fed into the cathode. Encouraged by a catalyst, the hydrogen atom splits into a proton and electron, which take different paths to the cathode. The proton passes through the electrolyte and the electrons create a separate current that can be utilized before they return to the cathode. In the porous electrode region, among the reactants, electrolyte, and catalyst there is a three-phase interface, which plays a critical role in the performance of the fuel cell. The electrolyte amount should be controlled carefully to avoid electrode flood, which causes loss of electrochemical performance.

Voltage output of a single fuel cell is not enough for most practical applications. For this reason, individual fuel cells are combined to produce acceptable voltage levels. A separator plate is used between the connected pairs to provide an electrical series connection between the cells and to provide a gas barrier that separates the fuel and oxidant of adjacent cells.

Figure 2 shows cell stacking. This figure is taken from Fuel Cell Handbook of DOE, 4th Edition.

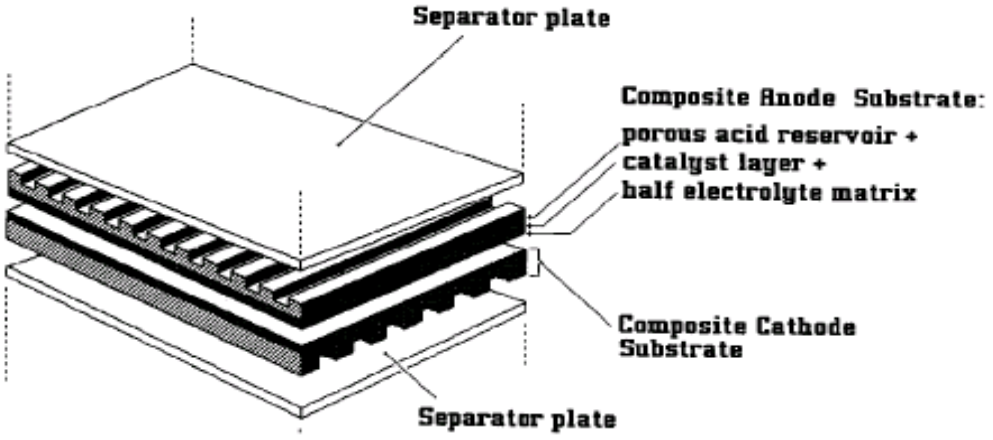


Figure 2 Schematic of a Cell Stack

A complete fuel cell plant consists of a fuel processor to obtain hydrogen from conventional fuels, stacks of fuel cell to produce energy, and a power conditioner unit that converts electrical power from dc to ac or regulated dc.

A schematic of a fuel cell plant is shown in Figure 3.

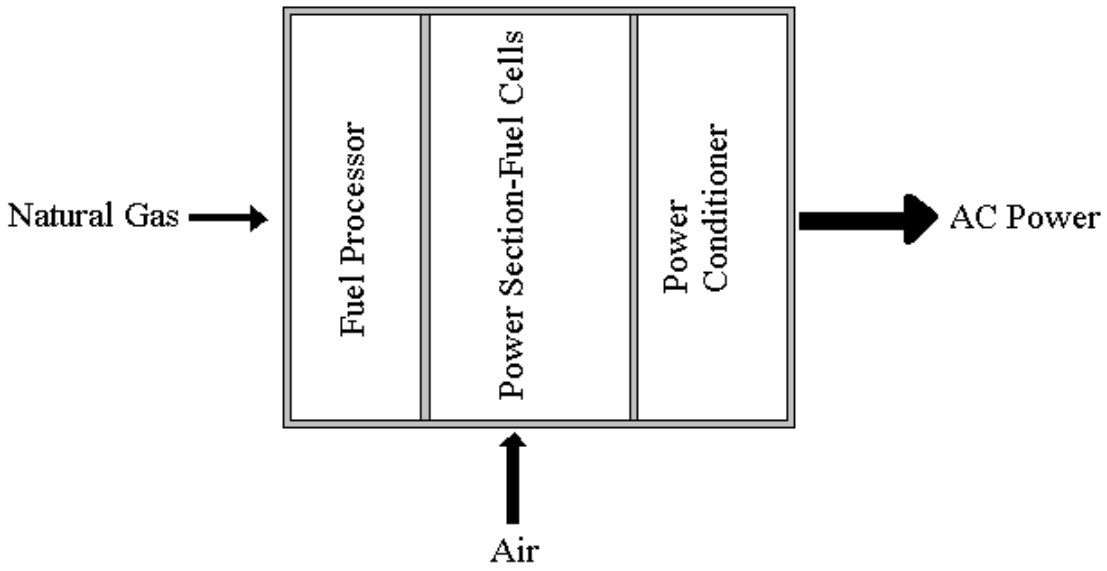


Figure 3 Schematic of a Fuel Cell Plant

## 2.3 Characteristics

Fuel cells can provide major environmental, energy and economic benefits. They convert the energy directly, so there is no combustion processes. The only emitted material from a fuel cell is water. Since there is no moving part, they are quiet and they have long operation life. Fuel cells offer efficiencies as high as 70% whereas the highest efficiency of a combustion engine is about 30%. Siting flexibility and fuel flexibility make the fuel cells compatible for many

applications. Remote operation is possible with fuel cells. They have rapid load following capability. Modular installation is possible with fuel cells, which gives them good size flexibility. Especially low temperature fuel cells have good reliability.

Besides these advantageous features, fuel cells also have some disadvantages. High initial cost is the most important problem associated with fuel cells. Lack of reliability and being an unfamiliar technology are the other main disadvantages of fuel cells.

## 2.4 Classification of Fuel Cells

Fuel cells can be classified as low temperature and high. They can also be classified as internal reforming and external reforming. The application areas of fuel cells create another classification such as mobile or stationary power stations.

But the most common classification of is by the type of electrolyte used in the fuel cell. Polymer electrolyte membrane (PEM) fuel cell, alkaline fuel cell (AFC), phosphoric acid fuel cell (PAFC), molten carbonate fuel cell (MCFC) and solid oxide fuel cell (SOFC) are the five main fuel cell types. The first three of them are considered low temperature fuel cells. Their operating temperatures are; ≈80°C for PEM, ≈100°C for AFC and ≈200°C for PAFC. The last two types are high temperature fuel cells. Their operating temperatures are, ≈650°C for MCFC, and ≈800-1000°C for SOFC. The operating temperature plays an important role in dictating the type of fuel that can be used in a cell. The low temperature fuel cells with aqueous electrolytes

are restricted to hydrogen as fuel. In high temperature fuel cells, CO and even CH can be used as fuel, since they are capable of internal reforming.

Among the five main types, alkaline fuel cell has been used only in space vehicles. The other four types have more application areas. A summary of the four different types, polymer electrolyte, phosphoric acid, molten carbonate and solid oxide fuel cells are given in Table 1. Data is taken from Fuel Cell Handbook, 4$^{th}$ Edition.

Table 1 Summary of the Fuel Cell Types

| | *PEM* | *PAFC* | *MCFC* | *SOFC* |
|---|---|---|---|---|
| Electrolyte | Ion Exchange Membrane | Immobilized Liquid Phosphoric Acid | Immobilized Liquid Molten Carbonate | Ceramic |
| Operating Temperature | $80^0$C | $205^0$C | $650^0$C | 800-$1000^0$C |
| Charge carrier | $H^+$ | $H^+$ | $CO_3^=$ | $O^=$ |
| External reformer | Yes | Yes | No | No |
| Prime components | Carbon based | Graphite based | Stainless steel | Ceramic |
| Catalyst | Platinum | Platinum | Nickel | Perovskites |

## 2.5 PEM Fuel Cells

Polymer electrolyte fuel cells basically have a proton conducting membrane sandwiched between two platinum impregnated porous electrodes. PEM fuel cell, like the solid oxide fuel cell, is one of the two fuel cell types, which have solid electrolytes.

### 2.5.1 Characteristics

The electrolyte in a PEM fuel cell is positively charged, which causes water to be produced at the cathode side. Polymer electrolyte fuel cell is a low temperature fuel cell. Typical operating temperatures are from 80°C to 120°C. Very high current densities are available from a PEM fuel cell. It has a fast start capability and a lightweight structure. Other advantageous points about this type of fuel cell are, there is no corrosive fluid hazard and the sensitivity to orientation is lower compared to the other types. These characteristics make PEM fuel cells best-suited type for vehicular power applications.

### 2.5.2 Performance

The electrochemical reaction that takes place in the fuel cell determines its ideal performance. For the PEM fuel cell, this electrochemical reaction is;

$$H_2 \longrightarrow 2H^+ + 2e^- \quad \text{Anode Reaction} \qquad (2\text{-}1)$$

$$1/2\,O_2 + 2H^+ + 2e^- \longrightarrow H_2O \quad \text{Cathode Reaction} \qquad (2\text{-}2)$$

The Nernst potential of the cell reactions defines the ideal performance. For an $H_2/O_2$ fuel cell, the ideal standard potential is 1.229 V. However actual performance of a fuel cell never achieves this value. There are always losses on the ideal performance, which are called polarization. There are three types of polarization losses. These are activation polarization, ohmic polarization and concentration polarization. Activation polarization occurs at low current densities. It is directly related to the rates of electrochemical reactions. Ohmic polarization occurs because of the resistance of the cell to the flow of ions. Decreasing the electrode separation and increasing the ionic conductivity can reduce ohmic losses. Concentration polarization occurs at high current densities. It is the loss of potential due to the inability of the surrounding material to maintain the initial concentration. Polarization losses can be calculated using the formulas below.

$$\eta_{act} = \frac{R \cdot T}{\alpha \cdot n \cdot F} \cdot \ln \frac{i}{i_0} \qquad \text{Activation Polarization Loss} \qquad (2\text{-}3)$$

$$\eta_{ohm} = i \cdot R \qquad \text{Ohmic Polarization Loss} \qquad (2\text{-}4)$$

$$\eta_{conc} = \frac{R \cdot T}{n \cdot F} \cdot \ln\left(1 - \frac{i}{i_L}\right) \qquad \text{Concentration Polarization Loss} \qquad (2\text{-}5)$$

where $\alpha$ is the electron transfer coefficient, T is the temperature, R is the universal gas constant, i is the current flowing through the cell, $i_0$ is the exchange current density, $I_L$ is the limiting current, R is the resistance of the fuel cell and F is Faraday's constant.

A wide range of performance levels can be obtained with PEM fuel cells. There are many parameters affecting the fuel cell performance. The structure and material of electrodes, electrolyte and catalysts are some examples. These can be considered as internal parameters.

There has been great effort on developing more economic and more efficient materials for these parts. Effects of different parameters on fuel cell performance are shown in Figure 4. Figure is taken from the Fuel Cell Handbook of DOE, 4th edition.

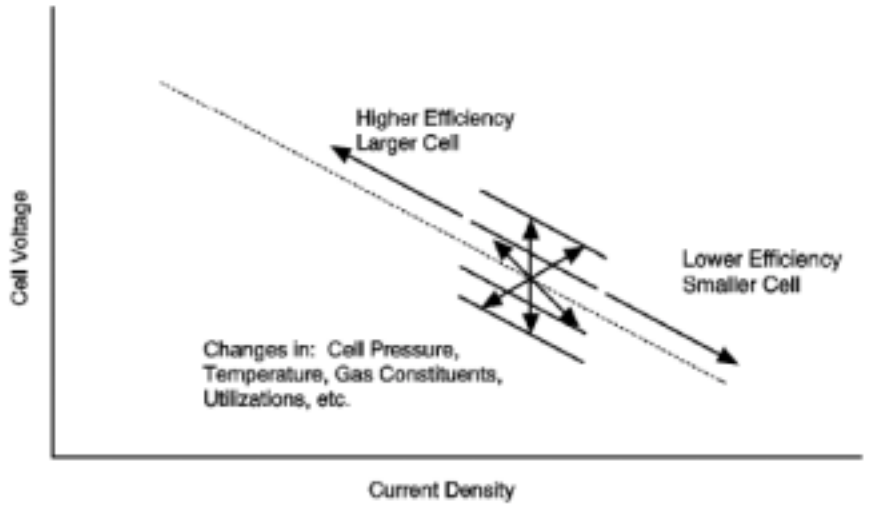


Figure 4 Effects of Parameters on Cell Performance

The operational parameters change cell performance. For example, increasing the operating temperature lowers the internal resistance of the cell and decreases the ohmic resistance. The result is an improvement in the cell performance. This improvement is limited by the vapor pressure of water in the ion exchange membrane. Thermal management of a fuel cell is very important and also has a great effect on cell performance. Operating pressure also has an influence on the PEM performance. An increase in the pressure leads to an increase in the performance of the fuel cell. Performance improvements due to pressure must be balanced against the energy required to increase the pressure. Figure 5, on the next page, shows the change in the cell voltage of a PEM fuel cell with the change in the $O_2$ pressure. Figure is taken from the Fuel Cell Handbook of DOE, 4th edition.

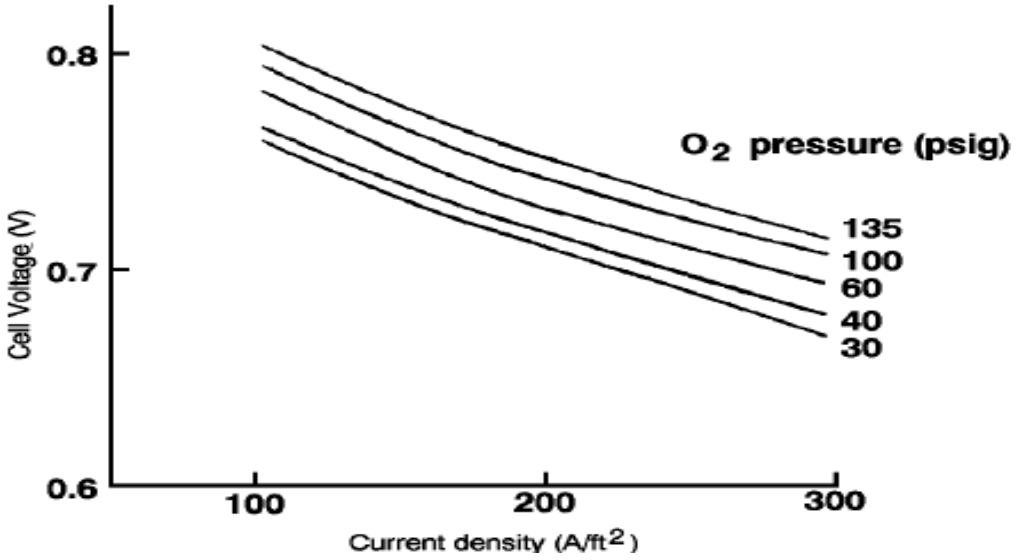


Figure 5 Influence of $O_2$ Pressure on Fuel Cell Performance

Water management also has a significant influence on cell performance. A high water content should be maintained in the electrolyte to obtain high ionic conductivity. The critical point is that, if more water is exhausted than produced, then it is important to humidify the incoming anode gas. However, if there is too much humidification, the electrode floods which causes problems. There are several methods used for water management such as capillary action, humidifying the incoming gas and employing temperature control between the inlet and the outlet.

# 3.0 MICROVALVES

## 3.1 General Information About Microvalves

As the industry's manufacturing requirements are increasing, new technologies are being developed to meet the challenging performance, cost, yield and reliability specifications. The field of microelectromechanical systems has been growing very fast in different fields. Microvalves are one of the widely used MEMS applications. With the advantages of reducing the internal volume, dead space, and contact surface area, decreasing system cost while improving performance and reliability in fluidic components, microvalves seem to have the potential to meet the requirements of fluidic devices.

A large number of microvalves have been demonstrated in the past. Terry et al in 1978 introduced the first silicon micro-machined valve. It was a solenoid plunger actuated micro-valve, used for injection in a gas chromatic air analyzer. In 1988, Park introduced a constant flow-rate micro-valve designed to operate with cerebrospinal fluid. The first micro-valve array system was proposed by Ohnstein et al. in 1990. The first commercially available micro-valve was produced in 1990's. From 90's to today, many microvalves are developed and produced for different purposes.

The application areas of the MEMS and micro-valve systems are growing constantly. Today, micro-valve systems are mainly used for micro-pump applications, process control, HVAC controls, test and calibration, biomedical dosing, chemical analysis systems and micro-

fluidic mixing. Besides, there are a big number of micro-valve systems developed just for a specific purpose like space applications. The microvalve design for fuel cell systems, the topic of this thesis, is another example of these kind of specific applications.

Most of the micro-valves have been micromachined from silicon. Silicon has many advantages for MEMS applications. It is one of very few materials that can be economically manufactured in single crystal substrates. (Maluf,N.,2000)* Its crystalline nature provides significant electrical and mechanical advantages. Besides, silicon is abundant and can be produced in high purity. It is an elastic and robust material. Good sealing properties make it the most used material for micro-valve applications. Especially spin-on silicone rubber is very attractive for microvalve applications since it has low modulus, high elongation, good compatibility with IC processes and good sealing properties. (Yang, X., 1999) Glass, polymers and thin metal films such as Ni, Ti, Fe, Cu are also used in micro-valve fabrication.

The basic structures of all micro-valves are similar. In general, these devices have stationary valve seat with inlet and outlet and a deflectable membrane. Deflection of the membrane opens or closes the valve according to its initial configuration which may be normally open or closed. The differences among the micro-valve systems are based upon geometry, actuation mechanisms, membrane material, flow path design and fabrication techniques. Among these differences, actuation is most commonly used property to classify the micro-valve systems.

* Parenthetical references refer to the bibliography.

For multi channel applications, micro-valve arrays are used. With micro-valve arrays, more precise flow is achievable since flow regulation is easier with an array than one valve. Another advantage of microvalve arrays is they also have a relatively low cost. (Vandelli, N., 1998)

## 3.2 Classification of Microvalves

The classification of microvalves can be made in three ways. According to the membrane material they can be classified as silicon-based and non-silicon-based microvalves. They can also be classified as normally open or normally closed microvalves according to their initial configuration. But the best method for classification is based on actuation. According to whether they have an actuator or not, micro-valve systems can be classified as active or passive. Active and passive microvalves have different characteristics and application areas.

### 3.2.1 Passive Microvalves

Passive micro-valves are simply check valves. These microvalve systems are mostly silicon based but some non-silicon based passive microvalves have also been produced. They are mainly used to block the flow in one direction. Passive microvalves are most commonly used in micro-pump applications. Very small leakage is required for passive microvalves. The response time, time that is the transition time during the open-to-close or close-to-open is another important parameter for the passive microvalve applications.

### 3.2.2 Active Microvalves

Active microvalve systems use actuators to regulate the flow and obtain the desired flow rate. Active microvalves are complicated systems compared to passive ones. There are multiple different actuation methods used in active microvalves.

There is no best actuation mechanism that fits all micro-valve applications, instead one should decide the best actuation according to system requirements. Parameters to be considered include: size, speed, ambient temperature, lifetime, electrical and thermal isolation, power consumption, manufacturing and proportional actuation requirements. Main actuation methods are piezoelectric actuation, electrostatic actuation, thermal actuation, electromagnetic actuation, shape memory alloy actuation, and pneumatic actuation. Making use of these methods, different actuation forces and mechanisms have been developed for microvalves. These methods and driving forces are explained in the following sections.

## 3.3 Actuation Methods and Mechanisms

### 3.3.1 Piezoelectric Actuation

Piezoelectric materials produce a charge when they are subjected to an external force. They also expand or contract in response to an externally applied voltage as illustrated in Figure 6. Piezoelectric actuation can provide large forces with low power consumption. However, the stroke is limited, requiring some sort of mechanical advantage.

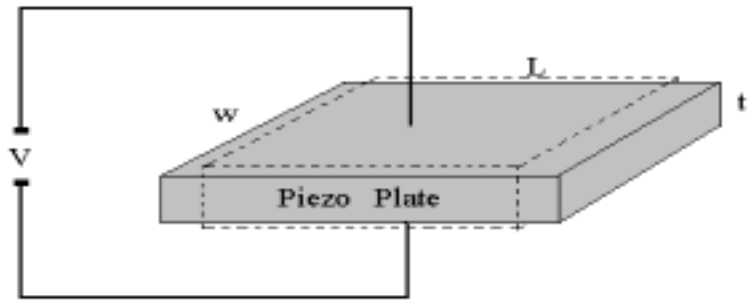


Figure 6 Illustration of the Piezoelectric Effect

When an external voltage V is applied across the thickness of a piezoelectric crystal, the displacements in the length ($\Delta L$), width ($\Delta W$) and thickness ($\Delta t$) are;

$$\Delta L = d_{31} \cdot V \cdot \frac{L}{t} \tag{3-1}$$

$$\Delta W = d_{31} \cdot V \cdot \frac{W}{t} \tag{3-2}$$

$$\Delta t = d_{33} \cdot V \tag{3-3}$$

In these equations, V is the applied voltage to the piezoelectric material, and $d_{31}$, and $d_{33}$ are the piezoelectric constants.

Axial and transversal piezoelectric actuators have high stiffness and they supply small movements and high forces. Previous piezo microvalve designs use stack actuation which is obtained by assembling large number of piezo layers together. Piezo stacks supply large forces and small deflections. For large deflections, piezoelectric actuators are usually used as bimorphs, where two layers of piezoelectric material are stacked so that the applied voltage causes one layer to contract and another to expand, thus providing more displacement. This method is used for the first time in a microvalve in this project.

### 3.3.2 Electrostatic Actuation

Electrostatic actuation uses electrostatic forces, which are the attractive forces between two plates or elements carrying opposite charges. An applied voltage, regardless of its polarity, results in an attractive electrostatic force. This actuation mechanism has many advantages for micro systems, including low power consumption with a very fast response time. Besides, although the electrostatic forces are low compared to some other actuation forces, since the parts in a micro system are approaching each other, electrostatic forces influence them effectively. (Hidenori, I., 1996)

When an external voltage $V$ is applied to parallel plates, the electrostatic force between them is;

$$F = \frac{1}{2} \cdot C \cdot \frac{V^2}{d} \tag{3-4}$$

Where;

$$C = \varepsilon_0 \cdot \varepsilon_r \cdot \frac{A}{d} \tag{3-5}$$

is the capacitance between the plates, $d$ is the spacing between the plates, $\varepsilon_0$ is the permittivity of the free space, $\varepsilon_r$ is the dielectric permittivity of the plates, $A$ is the area and $F$ is the electrostatic force.

### 3.3.3 Thermal Actuation

Thermal actuation consumes more power than electrostatic or piezoelectric actuation but it provides actuation forces on the order of hundreds of millinewtons or higher. For very small

structures, thermal actuation methods are more attractive. Bimetallic actuation and thermopneumatic actuation are examples of thermal actuation methods.

Bimetallic actuation capitalizes on the difference in the coefficients of thermal expansion between two joined layers of dissimilar materials to cause bending from a change in temperature. The generated pressure in bimetallic actuation is proportional to the difference between the thermal expansion coefficient of the two materials and the temperature change. As the temperature increases, one layer expands more than the other and activates the valve. This device is called thermal bimorph. An approximation for the radius of the curve of deflection for thermal bimorph is;

$$R = \frac{t_1 + t_2}{\varepsilon_1 + \varepsilon_2} \tag{3-6}$$

In this equation, $R$ is the radius of curvature of membrane deflection, $t_1$ is the thickness of the inner layer, $t_2$ is the thickness of the outer layer, $\varepsilon_1$ is the thermal strain of the inner layer and $\varepsilon_2$ is the thermal strain of the outer layer.

Thermopneumatic actuation uses a liquid that is heated inside a sealed cavity. Pressure from expansion or evaporation activates the valve. For thermopneumatic systems, generated pressure in the chamber is given by;

$$P = P_0 \cdot e^{-(L_0/R \cdot T)} \tag{3-7}$$

where $P_0$ is the initial pressure, $L_0$ is the latent of heat of vaporization, $R$ is gas constant and $T$ is absolute temperature.

### 3.3.4 Electromagnetic Actuation

Electromagnetic actuation has been a popular actuation method since the electromagnetic force can be controlled by the electric signals. (Hidenori, I., 1996)

Electrical current in a conductive element that is located within a magnetic field gives rise to an electromagnetic force in a direction perpendicular to the current and magnetic field. This force is called the Lorentz force, which is proportional to the current, magnetic field and length of the conductor. (Hidenori, I., 1996)

### 3.3.5 Shape Memory Alloy Actuation

The shape memory effect is a property of a special class of alloys. After being deformed by an external force, shape memory alloys return to their original shape when they are heated above their critical temperature. Shape memory alloys can simultaneously supply very large forces and the highest energy density available for actuation among all the actuation methods. On the other hand their response time is slower than other methods. Since they also require heat to actuate, shape memory alloy actuation can be considered as another type of thermal actuation.

### 3.3.6 Pneumatic Actuation

Pneumatic actuation needs external pneumatic actuators and a source of compressed air. They have the advantage of controlling the displacement and force over a wide range. The response time for pneumatic microvalves depends mainly on flow conductance of the tubing connection of the external valve to the micromachined elements in the system.

Miniaturization and complexity is a big problem for microvalves using this pneumatic actuation since this method needs relatively big pneumatic elements and an air supply.

### 3.3.7 Summary of Actuation Mechanisms

Six basic actuation methods and driving forces have been described in the previous section. Using these methods and forces, different actuation mechanisms can be produced.

The most common eight mechanisms that are used for microvalve applications are solenoid plunger application, piezoelectric actuation, pneumatic actuation, shape memory alloy actuation, electrostatic actuation, thermopneumatic actuation, electromagnetic actuation and bimetallic actuation. Six of them have the same name as the actuation method they use. The other two; solenoid plunger and bimetallic actuation mechanisms use magnetic and thermal actuation methods respectively.

Table 2, on the next page, compares the generated forces, maximum displacements, response times and reliabilities of the different actuation mechanisms. Depending on the applications requirements, the most suitable actuation mechanism can be selected considering the characteristics given in this table.

Table 2 Summary of the Characteristics of Actuation Mechanisms for MEMS (Shoji, S., 1998)

| Actuators | Force | Displacement | Response Time | Reliability |
|---|---|---|---|---|
| Solenoid Plunger | Small | Large | Medium | Good |
| Piezoelectric | Very large | Medium | Fast | Good |
| Pneumatic | Large | Very Small | Slow | Good |
| SMA | Large | Large | Slow | Poor |
| Electrostatic | Small | Very small | Very Fast | Very Good |
| Thermopneumatic | Large | Medium | Medium | Good |
| Electromagnetic | Small | Large | Fast | Good |
| Bimetallic | Large | Small | Medium | Poor |

# 4.0 DESIGN AND SPECIFICATIONS

## 4.1 Problem Definiton

In the previous sections, performance characteristics of PEM fuel cells are reviewed. We have seen that many parameters can make a difference in the fuel cell performance. In addition, new problems associated with poor distribution of reactant fuel across the membrane surface arise when fuel cells stacked together. Condensation of water vapor onto the channel surfaces causes problems by blocking the flow and restricting the amount of hydrogen reacting with catalyst. This decreases the reaction rate and the voltage output. On the other hand, excess reactant flow is also a problem since it decreases the overall efficiency of the cell. These situations can arise at different operating points for a stack depending on the temperature, pressure, anode, cathode flow rates and power draw from the stack. If the stack is operated under these conditions for a long time, damage can occur. Therefore, reactant flow must be controlled carefully and with high precision to avoid performance loss or damage.

For a fuel cell to achieve an optimal performance it is important that the electrochemical reaction be evenly distributed over the cell surface. If that is not achieved, various debilitating effects arise, including poor fuel-to-electric efficiency, hot spots which lead to shorter stack lifetimes, or simply lower output voltages at a given load.

## 4.2 Proposal

For all the reasons explained above, non-homogeneous distribution of reactants should be avoided to maximize the fuel cell performance. MEMS technology seems to have the potential to overcome this flow problem in fuel cell stacks. MEMS based micro-fluidic devices offer opportunities to achieve increased performance and higher levels of functional integration, at lower cost with decreased size and increased reliability for fluid control and distribution. A piezoelectrically driven micro-valve or microvalve stack placed in the entrance of the hydrogen channels is proposed to vary the hydrogen flow rates in response to the changes in the output. Piezoelectric actuation seems to be the best choice because of its fast response time, low power consumption and ease of fabrication. Magnetic actuation could be another choice of actuation but the complex nature of magnetic actuation mechanisms brings difficulty in fabrication and increases cost.

Each microvalve or microvalve stack will be placed internally at the entrance of the eleven hydrogen-carrying channels instead of placing one microvalve in each of eleven hydrogen channels. This will reduce cost and give more flexibility in design in terms of dimensional considerations. The working principle of the normally open microvalves can be explained as follows: As voltage decreases, microvalves will open and provide more flow to the cells to increase the voltage back to its original value. On the other hand, if the voltage decreases, microvalves will close and decrease the flow rate to decrease the voltage back to its original value. A proportional control method will be developed and used to control the microvalve operation.

Figure 7 illustrates the microvalve stack placement in the entrance of hydrogen channels. The entrance of the hydrogen channels is originally a circular section which apperas as two semi-circles in the figure, after the microvalve stack is placed.

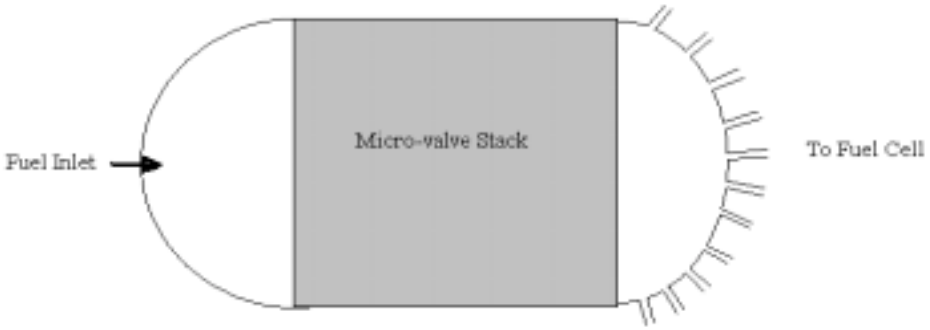


Figure 7 Schematic of Microvalve Stack Assembly

### 4.3 Physical Design

Main considerations for this microvalve design include ambient temperature, pressure difference, required flow rate, dimension restrictions and environmental effects. PEM fuel cells operate between 80°C and 120°C. A maximum temperature difference of 80°C is used in calculations since the initial temperature is taken as room temperature which is 25°C. Desired pressure difference and the flow rate per cell are 1 Psi and 0.441 Slpm respectively. Dimensions for the microvalve or microvalve stack should be kept below $1 \times 1 \times 0.09375$ inches and there is no restrictions for the number of microvalves. Finally, the most important environmental concern is the hydrogen embrittlement problem. Hydrogen can cause different types of cracks in many metals and materials. This problem can be mitigated either by selecting a resistive material or a applying a proper coating on any material.

Figure 8 gives the cross-sectional view of the microvalve parts. The microvalve looks like a rectangular plate. It has overall dimensions of 22.7 mm in length, 20 mm in width and 1 mm in thickness. The flow channel, which is etched in the upper wafer, has a height of 30 μm and a width of 4 mm. With these dimensions two microvalves can be placed in the flow channel entrance which will help reducing the flow velocity in the flow channels since there will be less flow rate per channel. The middle wafer shields the actuator from flow and pressure forces. A thin channel is left under the actuator in the bottom wafer to avoid sticking the actuator to the membrane. The actuator is located on the lower part. There is a rectangular gap with an area of 220 × 4020 μm on this part to allow the gate movement on the actuator to open and close the valve. This configuration helps decrease the total force on the actuator since using the gate decreases the area subjected to the pressure drop across the valve. The gate is on the tip of the bender and with a given voltage the bender pushes it up through the gap in the middle membrane part into the flow channel to close the valve.

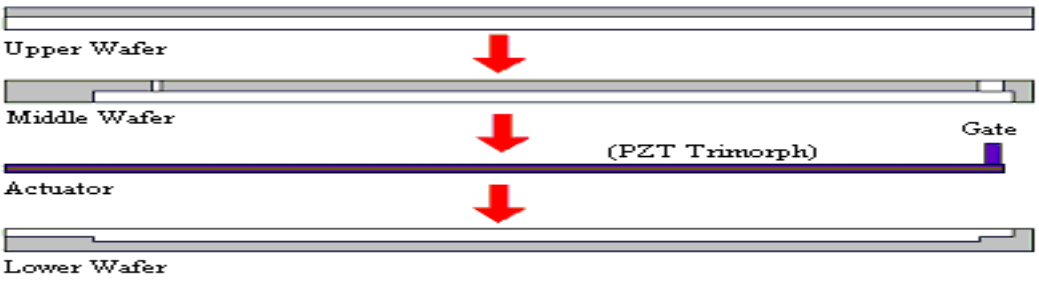


Figure 8 Microvalve Parts

There are a total of four parts in the microvalve. The actuator part is a 22.5 mm × 4mm × 290 μm cantilevered trimorph piezoelectric bender. It is made of a brass sheet sandwiched between two lead zirconate titanate PZT 5-H type piezo sheets. A glue layer attaches the bender

to the lower membrane part. 2 mm of the actuator is used for this bonding. Another 0.5 mm extends outside the valve for electrical connections. The remaining 20 mm part does the actuation. A 200 μm high 210 μm thick and 4 mm wide brass gate near the tip of the bender is used to close the valve.

The main reason for using a parallel trimorph structure for the actuator is to eliminate the bimorph thermal effects on the displacement of the bender. If two solids of different thermal expansion coefficients are glued together and heated the structure will bend to one side and this is called bimorph thermal actuation. Having piezo layers on both sides eliminates this effect since they have the same thermal expansion coefficient. Otherwise, if a piezo-brass bimorph were used, for example, thermal bimorph actuation creates much bigger displacement than piezoelectric actuation. A temperature change as small as 20 degrees would eliminate or double the displacement of the bender and make it impossible to control.

The other parts of the microvalve are made of silicon. There are wafers and they all have the same width and length of 20 mm and 22.2 mm respectively. They are mainly rectangular blocks with some parts etched away either to form the flow channel or to form the actuator bed. Minimum wall thickness of all three parts is 0.5 mm.

There is a small hole on the middle membrane part to equalize the pressure of the inlet and the pressure around the bender. Having the same pressure on both sides of the bender means here is no pressure induced force on the bender so that it can give the highest possible displacement for an applied voltage.

## 4.4 Analysis

### 4.4.1 Electromechanical Analysis

In the electromechanical analysis section, two different analyses are performed. The first one is the deflection analysis to find the bender displacement for a specified voltage and the second is the strength analysis to find out if the design fails under maximum loading conditions. Both analyses were performed using the finite element analysis software ANSYS 5.7.

Material properties used for modeling are listed in Table 3. Data for PZT-5H type piezo sheets is taken from Piezo Systems Inc., Cambridge,MA.

Table 3 Material Properties

| Material Property | Lead Zirconate Titanate | Brass |
|---|---|---|
| Modulus of Elasticity, Pa | $6.6 \times 10^{10}$ | $16 \times 10^{10}$ |
| Poisson's Ratio | 0.33 | 0.34 |
| Density, $kg/m^3$ | 7800 | 8543 |
| Relative Permittivity | 1800 | ------ |

The element types for piezo and brass sheets are selected as ANSYS coupled field element 5 and brick element 45, respectively. Displacements in *x*, *y* and *z* coordinates and voltage are set as degrees of freedoms for coupled field element 5 in the free deflection analyses.

A parametric study on voltage levels, layer thickness and plate areas was conducted to determine how the changes in these parameters affect the maximum tip displacement. These studies are done find the best solution in terms of displacement, strength, elasticity and ease of fabrication of the bender. To obtain the maximum bender displacement, after drawing and meshing the actuator in ANSYS, a voltage of 10 Volts applied to both piezo layers. A mesh size of 500 μm is used and parts are glued using mesh convergence. Table 4, Table 5 and Table 6 summarize these results. The numbers represent the deflection of the trimorph structure without the gate. Analysis of the actuator with the gate are performed and presented in the later sections.

Table 4 Maximum Bender Deflection with Variable Voltage

| PZT Thickness | Brass Thickness | Length | Width | Voltage | Max. Deflection |
|---|---|---|---|---|---|
| 100 μm | 25 μm | 20 mm | 20 mm | 1 V | 12.4 microns |
| 100 μm | 25 μm | 20 mm | 20 mm | 2 V | 24.8 microns |
| 100 μm | 25 μm | 20 mm | 20 mm | 5 V | 62 microns |
| 100 μm | 25 μm | 20 mm | 20 mm | 10 V | 124 microns |

Figure 9, on the next page, gives the same relation in graphical form. It is clear from the graph that the relation between voltage and deflection is exactly linear once the deflection is calculated for a specified voltage, then it is possible to find the deflection of the bender for any voltage level. This diagram is commonly called the voltage-deflection diagram for a piezoelectric device.

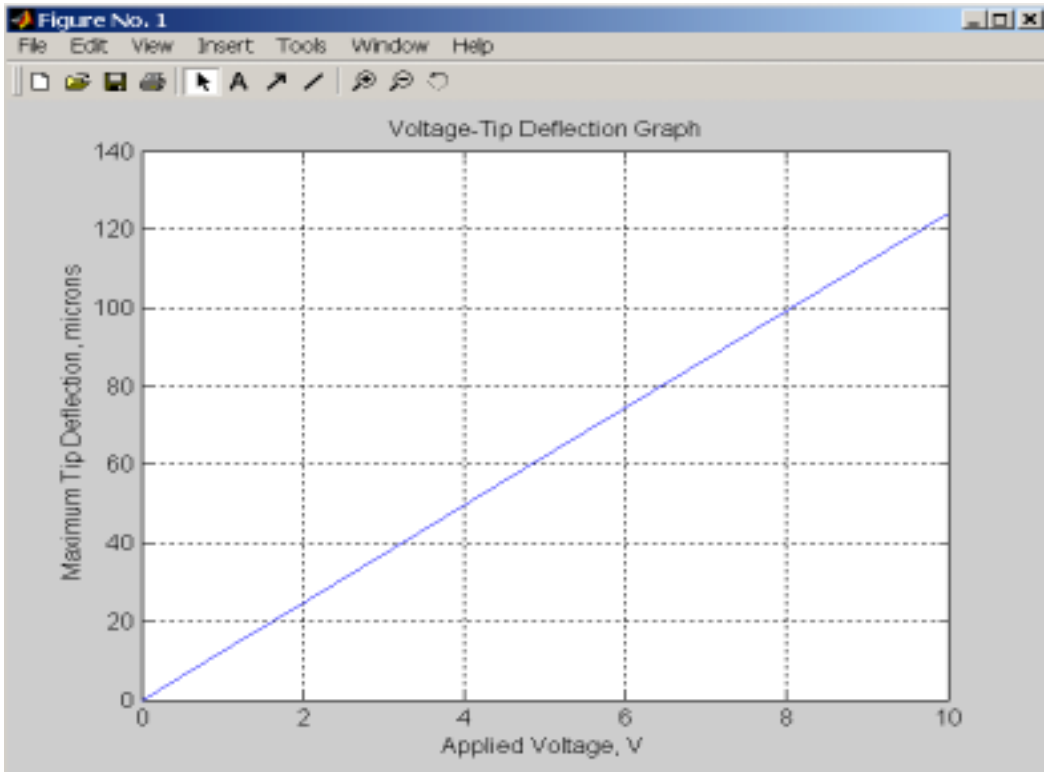


Figure 9 Voltage Deflection Relation

Table 5 gives the maximum bender deflection values for 100 μm thick piezo layers and different thickness values for brass layer. The "0" μm thick means PZT/PZT bimorph actuator.

Table 5 Maximum Bender Deflection with Variable Brass Layer Thickness

| PZT Thickness | Brass Thickness | Length | Width | Voltage | Max. Deflection |
|---|---|---|---|---|---|
| 100 μm | 0 μm | 20 mm | 20 mm | 10 V | 142 microns |
| 100 μm | 25 μm | 20 mm | 20 mm | 10 V | 124 microns |
| 100 μm | 50 μm | 20 mm | 20 mm | 10 V | 108 microns |
| 100 μm | 75 μm | 20 mm | 20 mm | 10 V | 93.1 microns |
| 100 μm | 100 μm | 20 mm | 20 mm | 10 V | 80.2 microns |

Table 6 gives the maximum bender deflection values for 25μm thick brass layer and different thickness values for the piezo layers. The 127 μm and 191 μm are standard element thicknesses that can be purchased from Piezo Systems, Inc., Cambridge, MA.

Table 6 Maximum Bender Deflection with Variable Piezo Layer Thickness

| PZT Thickness | Brass Thickness | Length | Width | Voltage | Max. Deflection |
|---|---|---|---|---|---|
| 25 μm | 25 μm | 20 mm | 20 mm | 10 V | 1287 microns |
| 50 μm | 25 μm | 20 mm | 20 mm | 10 V | 432 microns |
| 75 μm | 25 μm | 20 mm | 20 mm | 10V | 211 microns |
| 100 μm | 25 μm | 20 mm | 20 mm | 10 V | 124 microns |
| 127 μm | 25 μm | 20 mm | 20 mm | 10 V | 70.6 microns |
| 191 μm | 25 μm | 20 mm | 20 mm | 10 V | 19 microns |

Figure 10 graphically depicts information from Table 5 and Table 6. From the tables and figures, it can be seen that the maximum deflection changes linearly with voltage. It also increases by increasing the width or length i.e. the area of the plate since the resulting piezoelectric force gets larger. Keeping all the other parameters constant, increasing the thickness of any layer decreases the maximum deflection since it increases the spring force against deflection. Increasing the thickness of piezo layers has a more significant effect on bender deflection than increasing brass thickness. Although having thin piezo layers produces very good deflection results, 127 μm layers are used for the microvalve instead of 25 μm or 50 μm ones since piezoelectric ceramics are very brittle materials and decreasing the thickness increases the risk of failure and makes the microvalve harder to fabricate. Another advantage of

using 127 μm piezo layers is that they are already commercially available and this eliminates the need for polishing piezo layers to make them thinner and reduces the fabrication time.

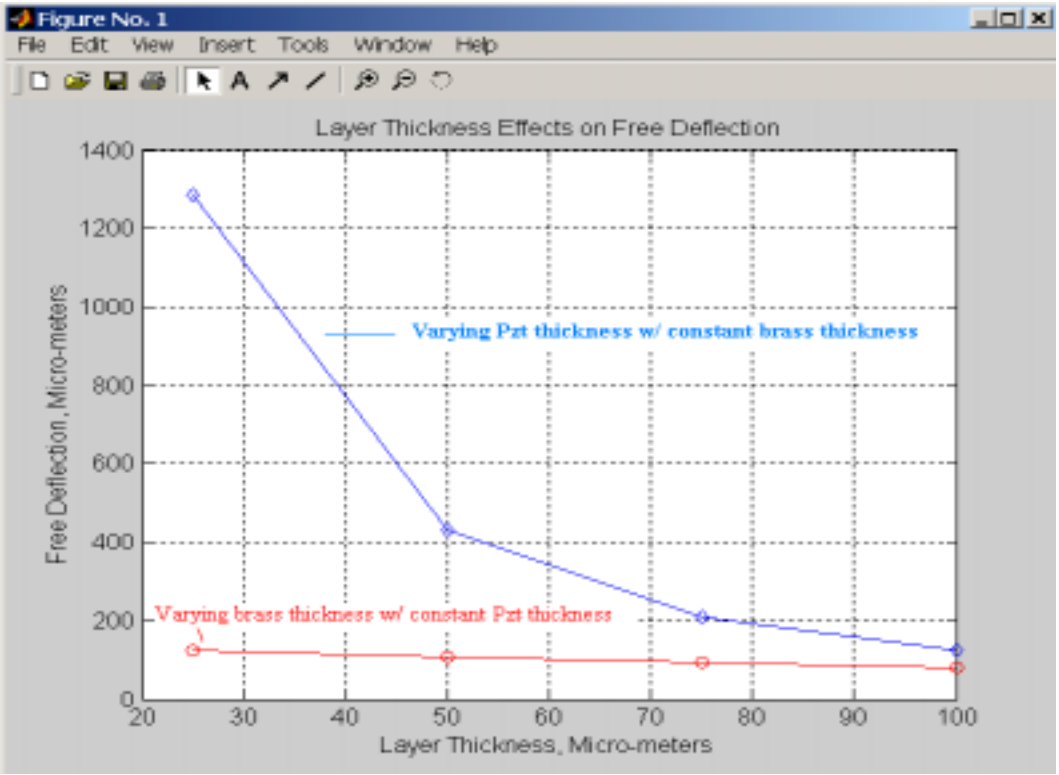


Figure 10 Relation Between the Layer Thickness and Free Bender Deflection

The next step in electro-mechanical analysis is to find out the changes in the deflection when the valve gate is mounted on the bender. ANSYS models of the trimorph with the gate for different dimensions are developed for this purpose and deflection and stress analysis are performed on these models. Only results for a 4 mm wide and 20 mm long bender are presented since these are the dimensions of the final design. When modeling the actuator with the gate, it is important to select mesh size properly. The nodes that are defining the base of the gate must be exactly at the same locations with the nodes that are defining the bender at that region.

Otherwise, ANSY treats the gate and bender as separate parts. In other words, there shouldn't be any extra nodes on the bender to define gate base on the piezo plate. Therefore, the structure is re-meshed with a mesh size of 200 μm. Adding the gate changes the displacement values and distribution over the tip of the bender. The maximum displacement under 10-Volt excitation decreases from 64.1 μm to 64 μm after the gate is bonded on the bender. On the other hand, it makes the tip of the bender more rigid, and helps keep the shape of the bender tip straight, countering the Poisson effects, since length to width ratio is 5. Although the non-uniformity of the tip does not show up for the current 4mm wide design, it becomes clearly visible when the width increases i.e. the bender becomes more like a plate. Figure 11 shows the bender deflection before the gate is mounted.

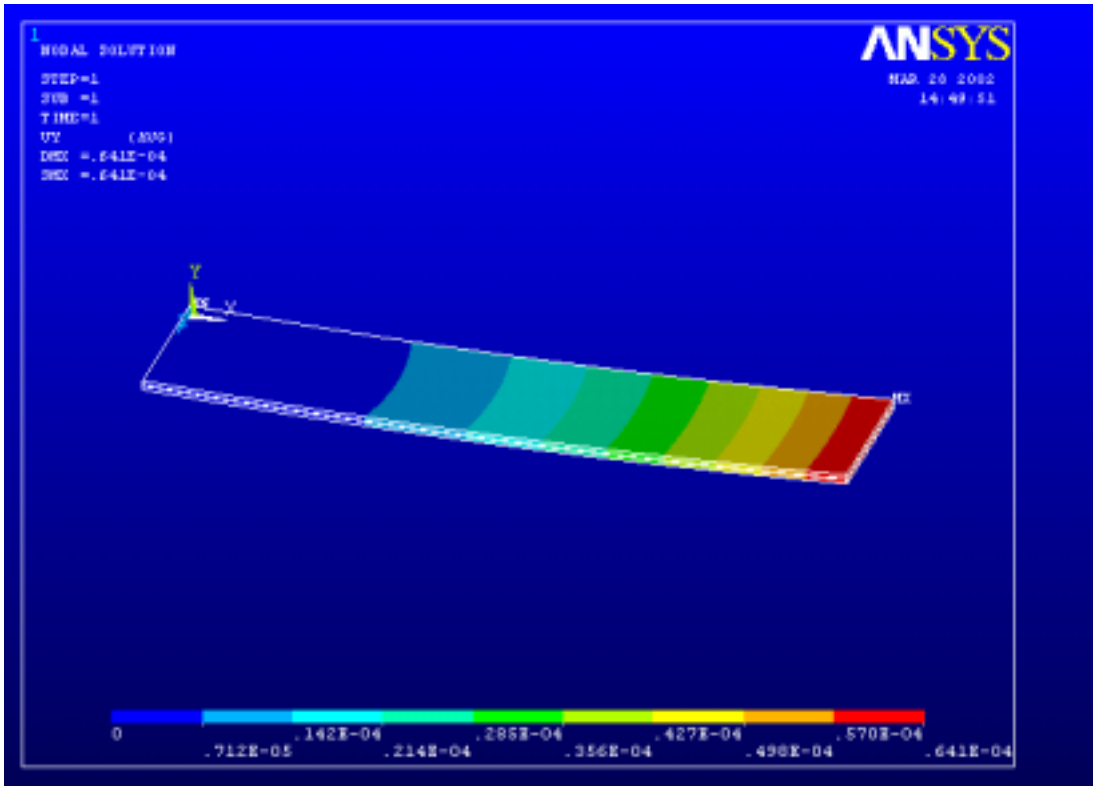


Figure 11 Free Deflection of 4 mm × 20 mm Trimorph with no Gate

Figure 12 and Figure 13 show the free bender deflection and the 3D view of the deformed and undeformed shapes after the gate is mounted.

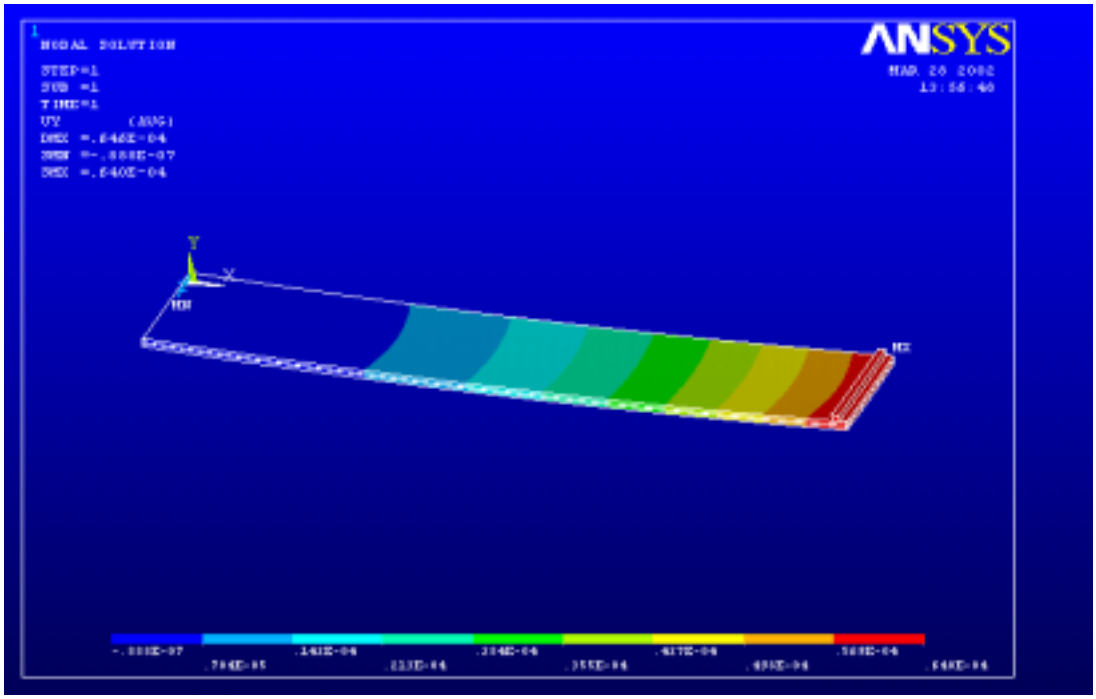


Figure 12 Free Deflection of the 4mm Wide Bender after the Gate is Mounted

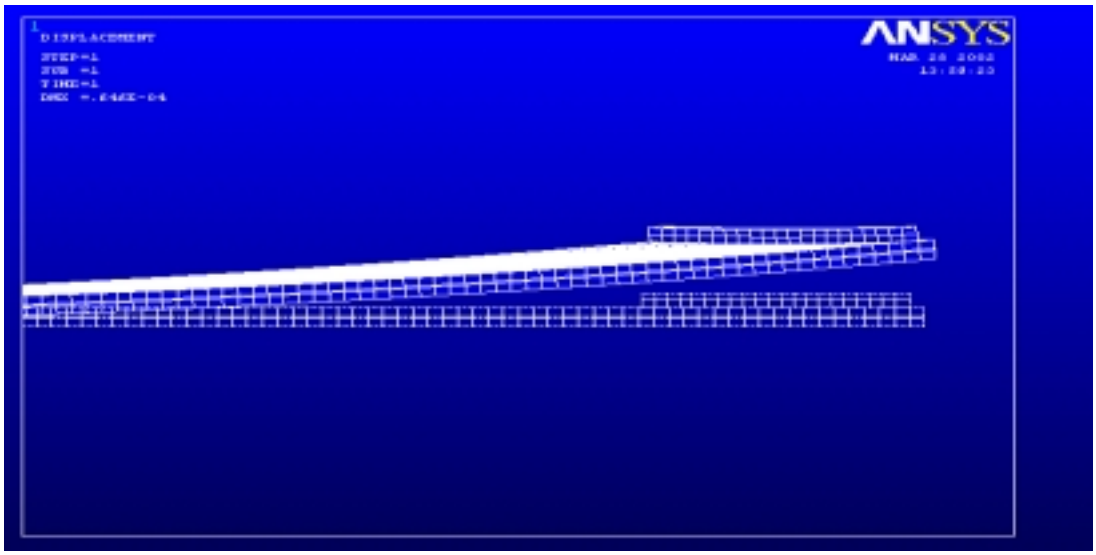


Figure 13 Deformed and Undeformed Shapes of the Bender

To demonstrate the non-uniform deflection and the effects of valve gate more clearly, a wider bender with dimensions 20 mm × 20 mm is modeled. Figure 14 shows the free deflection of this trimorph without the valve gate. It is clear that not all points on the tip have the same deflection value. Corners deflect more than the central parts by a margin of almost 10 μm as a result of Poisson effect, which is not desirable for both flow control and structure strength points of view.

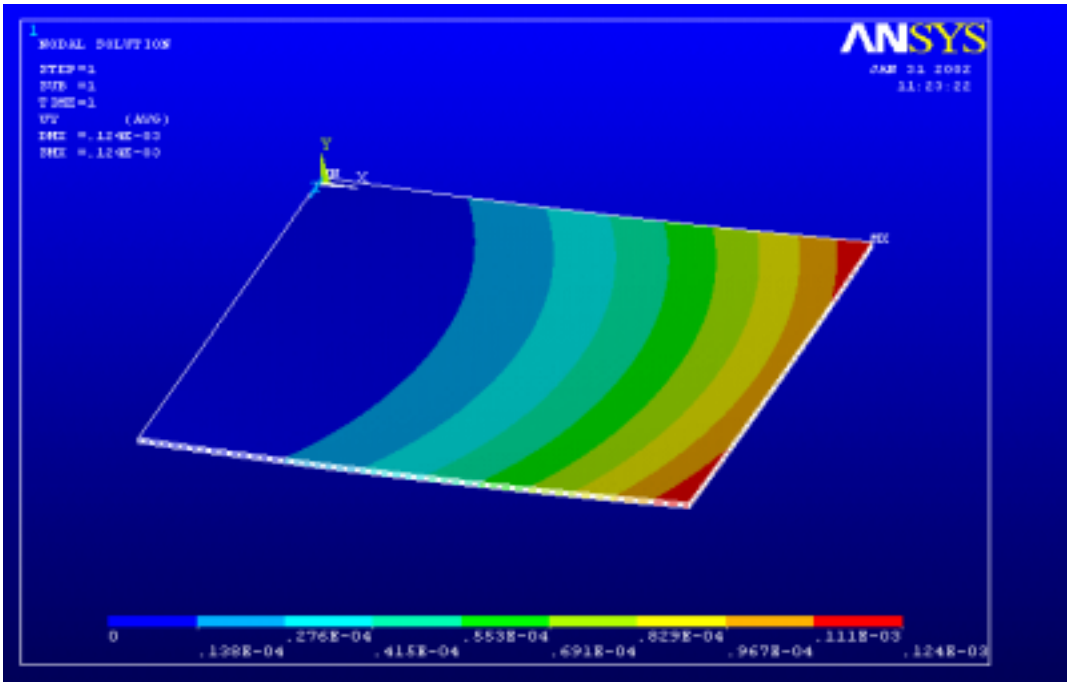


Figure 14 Free Deflection of 20 × 20 mm Trimorph Bender without the Valve Gate

Figure 15 on the next pages shows the deflection for the same bender after the gate is mounted. In this case the tip deflection decreases from 124 μm to 120 μm but all the points at the tip deflects 120 μm.

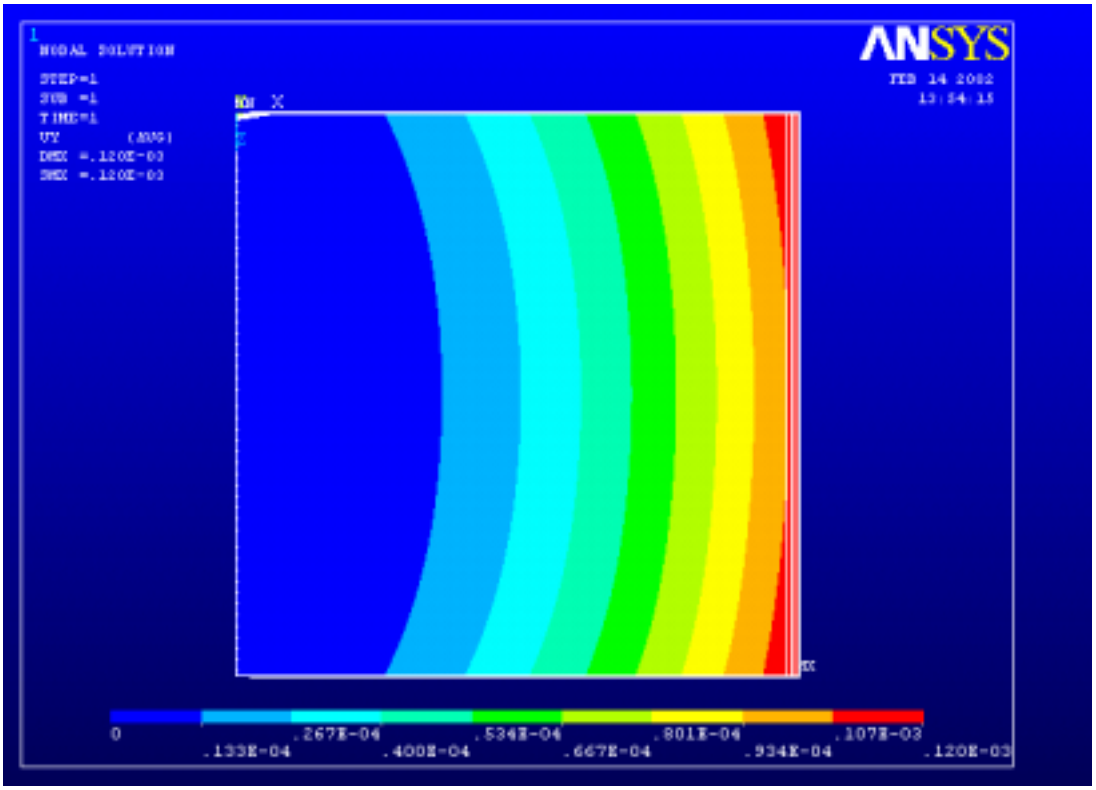


Figure 15 Deflection of the Bender with the Gate Mounted

Mounting the gate not only changes the deflection characteristics but also changes the maximum stress and stress distribution over the bender. Von Misses stresses are evaluated for failure criteria. Before the gate is mounted, a maximum stress of 6.22 MPa occurs at the cantilever edges and the minimum stresses occur at a place near to the cantilever end. After the gate is mounted, maximum stress level increases to 6.39 MPa and it occurs on the valve gate. The minimum stress area remains at its location but there exists one more minimum stress area located very close to the valve gate. Figure 16 and Figure 17 show the Von Misses stress distributions on the $4 \times 20$ mm trimorph before and after the gate is mounted respectively. Since the failure strength of PZT and brass are 63 and 270 MPa, a factor of safety of 10 is achieved in the device for 10 Volts excitation without the thermal and fluidic forces.

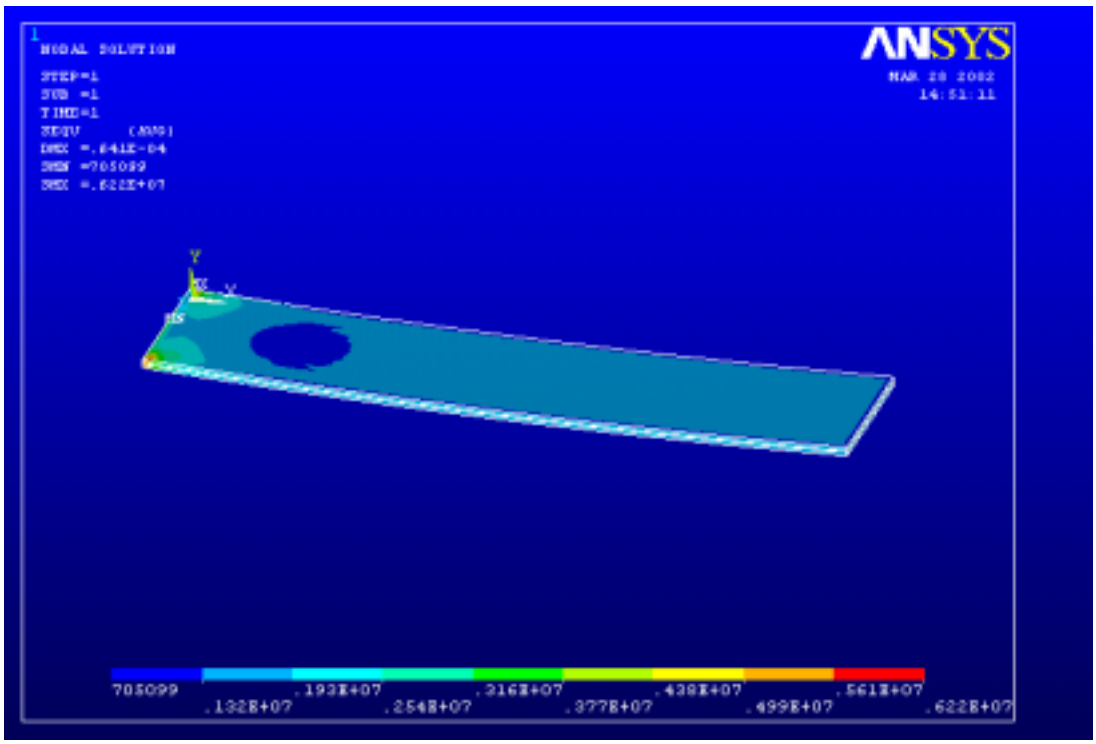


Figure 16 Von Misses Stress Distribution before the Gate is Mounted

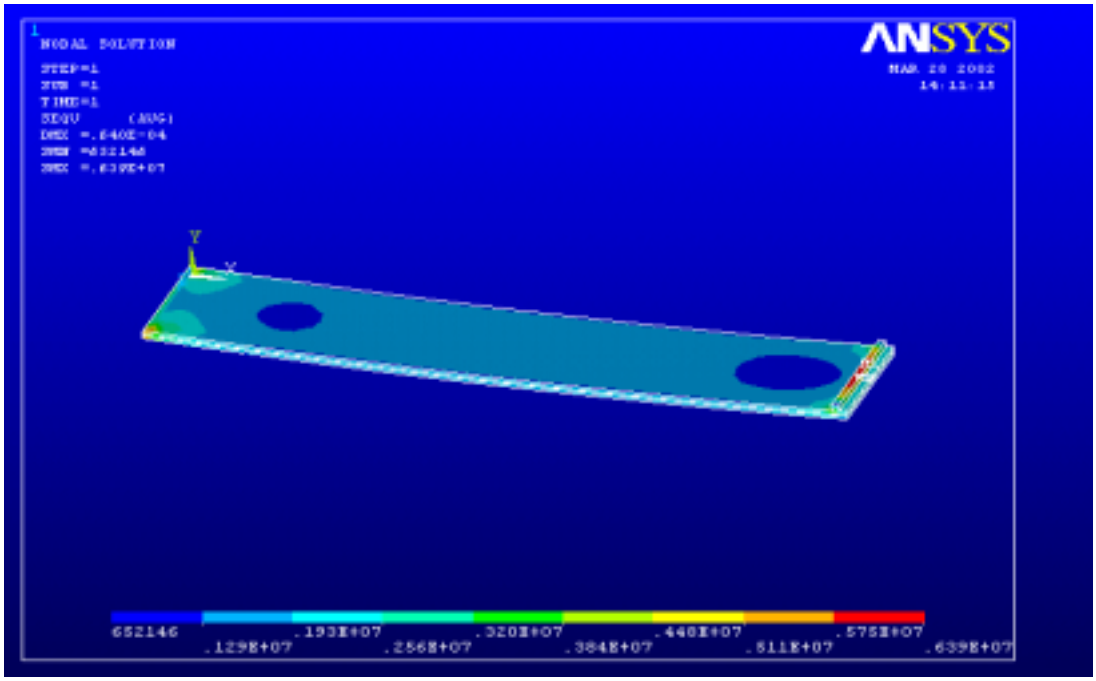


Figure 17 Von Misses Stress Distribution after the Gate is Mounted

### 4.4.2 Fluidic Analysis

Fluidic analysis of the microvalve includes flow rate, velocity, drag force calculations, and pressure drop. The microvalve design is optimized according to the results. Width and channel height of the microvalve are kept at a minimum where the microvalve can still supply the required flow rate with an acceptable velocity and resulting forces.

The NETL fuel cell requires a flow rate of 0.44 L/min at maximum power, which corresponds to $7.4\times10^{-6}$ $m^3$/sec. Since there are two microvalves used per cell, the maximum flow rate in each microvalve is $3.7\times10^{-6}$ $m^3$/sec. To decide the final dimensions of the microvalve, velocity and force calculations are done with many different width and thickness combinations using MATLAB and ANSYS. Changing the width of the flow channel means a change in the width of the actuator also. This results in a change in maximum deflection of the actuator, which brings a change in flow channel height. So, for a specified value of channel width, there is only one maximum channel height that can be determined by the maximum deflection of the actuator at the given operating voltage. The final design geometry was chosen to be 4 mm wide, 30 μm high with the operating voltage of 5 Volts. This combination is a good optimization in terms of both keeping the dimensions small and working with a low voltage.

The cross sectional area, $A$, of the flow channel is $12\times10^{-8}$ $m^2$. The velocity, $V$, in the flow channel can be calculated by dividing the flow rate by the cross-sectional area,

$$V = \frac{Q}{A} \tag{4.1}$$

The resulting flow velocity is calculated to be 30.6 m/sec. which is not excessive for hydrogen gas. Properties of the flow in the microvalve are summarized in Table 7. Knudsen number, *Kn*, which is one of the properties given in Table 7, is a key non-dimensional parameter for gas micro flows. I is defined as the ratio of the mean free path, $\lambda$, over a characteristic geometry length, *L*. For a fluid, appropriate flow and heat transfer models depend on the range of the Knudsen number. If it is less than 0.01, than the fluid is considered as continuum while for Knudsen numbers higher than 10, it is considered as a free molecular flow. The Knudsen number is calculated using Reynolds, *Re*, and Mach, *Ma*, number as follows, (Karniadakis, G., 2002)

$$Kn = \frac{\lambda}{L} = \sqrt{\frac{\gamma \cdot \pi}{2}} \cdot \frac{M}{\mathrm{Re}} \tag{4.2}$$

$$\mathrm{Re} = \frac{\rho \cdot V \cdot D_h}{\upsilon} \tag{4.3}$$

$$Ma = \frac{V}{C} \tag{4.4}$$

$$D_h = \frac{2 \cdot w \cdot h}{(w + h)} \tag{4.5}$$

where $\rho$ is the density, $\nu$ is the viscosity, $D_h$ is the hydraulic diameter, and $\gamma$ is the temperature constant of the fluid and C is the sound of speed.

Table 7 Properties of Hydrogen Flow

| | |
|---|---|
| Flow Rate per microvalve (Q) | $3.7\times10^{-6}$ $m^3$/sec |
| Flow Area (A) | $12\times10^{-8}$ $m^2$ |
| Velocity (V) | 30.6 m/sec |
| Mach Number (Ma) | 0.02 |
| Reynolds Number (Re) | 14.5 |
| Knudsen Number (Kn) | 0.0021 |

From the Reynolds, Mach and Knudsen numbers the appropriate flow model can be explained as incompressible and laminar flow in the continuum regime.

The flow will apply a drag force on the valve gate. Drag force is a function of area of the flow and the square of the flow velocity. This drag force will effectively create a moment on the actuator, $M_D$, and this moment can be replaced by an equivalent vertical force on the valve gate, $F_{ver}$. Figure 18 shows the drag force and the resulting equivalent moment and vertical force on the tip of the actuator.

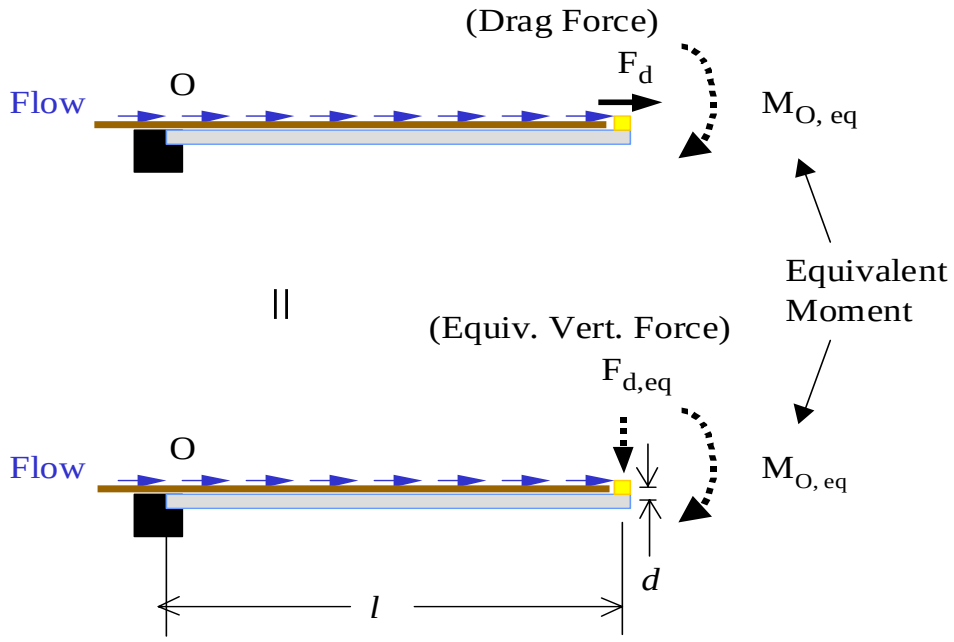


Figure 18 Drag Force and Moment and the Equivalent Force on the Actuator

Drag force, $F_D$, can be calculated from:

$$F_D = \frac{1}{2} \cdot C_D \cdot \rho \cdot A \cdot V^2 \tag{4.6}$$

where $C_D$ is the drag coefficient which was chosen to be 2.5 to include a factor of safety. The velocity will increase when the valve is partially closed. To be safe in all conditions, the drag force is very conservatively calculated for the worst case scenario i.e. for a 4 mm×30 μm flow channel with a flow velocity of 10 times the average velocity. The resulting drag force on the gate is calculated to be 985 μN. This force creates an equivalent moment around point O on the actuator, which can be calculated from,

$$M_{D,eq} = F_D \cdot d \tag{4.7}$$

where $d$ is the vertical distance from the centroid of the distributed drag force to the neutral axis of the bender. $M_{D,eq}$ is calculated to be 33 μN-m. To find the equivalent vertical force, the following equation can be used.

$$M_{D,eq} = M_{F_{D,eq}} = F_{D,eq} \cdot l \tag{4.8}$$

where $F_{D,eq}$ is the equivalent vertical force and $l$ is the free length of the cantilever bender which is 20mm. From this equation the vertical force is calculated as 16 μN.

There is one more force acting on the actuator associated with the flow. This force is caused from the pressure difference between the both sides of the valve gate. This pressure force, $F_P$, is also in the direction of drag force and it can also be replaced by a vertical equivalent force using the same method above. Pressure force is a function of pressure difference and area and it can be calculated from,

$$F_P = \Delta P \cdot A \tag{4.9}$$

where $\Delta P$ is the pressure drop across the gate. For the maximum pressure difference of ΔP=1 Psi, the pressure force is calculated as 830 μN. The resulting moment on the tip of the bender, $M_{P,eq}$, is 0.27 μN-m. Equivalent vertical force can be calculated from;

$$F_{P,eq} = \frac{M_P}{d} \tag{4.10}$$

The vertical equivalent of the pressure force is calculated to be 14 μN. The total vertical force on the bender can be calculated using,

$$F_{total} = F_{D,eq} + F_{P,eq} \tag{4.11}$$

The total vertical force is calculated to be 30 μN. The summary of the fluidic forces on the actuator is given in Table 8. These forces, together with thermal forces, are used to find the exact operating point of the actuator and to find the tip deflection at that point.

Table 8 Summary of Fluidic Forces on the Bender

| Force Type | Magnitude |
|---|---|
| Drag Force ($F_D$) | 985 μN |
| Equivalent Vertical Drag Force ($F_{ver}$) | 16 μN |
| Pressure Force ($F_P$) | 830 μN |
| Equivalent Vertical Pressure Force ($F_{ver2}$) | 14 μN |
| Total Vertical Fluidic Force on the Bender | 30 μN |

To find the operating point, first the blocked force for the bender under 5-Volt excitation is calculated as $7.3\times10^{-3}$ N using ANSYS. Different force values are applied to the trimorph and the force, that causes a deflection of the same magnitude with the free deflection is taken as the blocked force. Figure 19 shows the ANSYS result. After calculating the blocked force, the force-deflection diagram of the actuator can be drawn. The diagram is drawn using MATLAB. Figure 20 shows MATLAB figure.

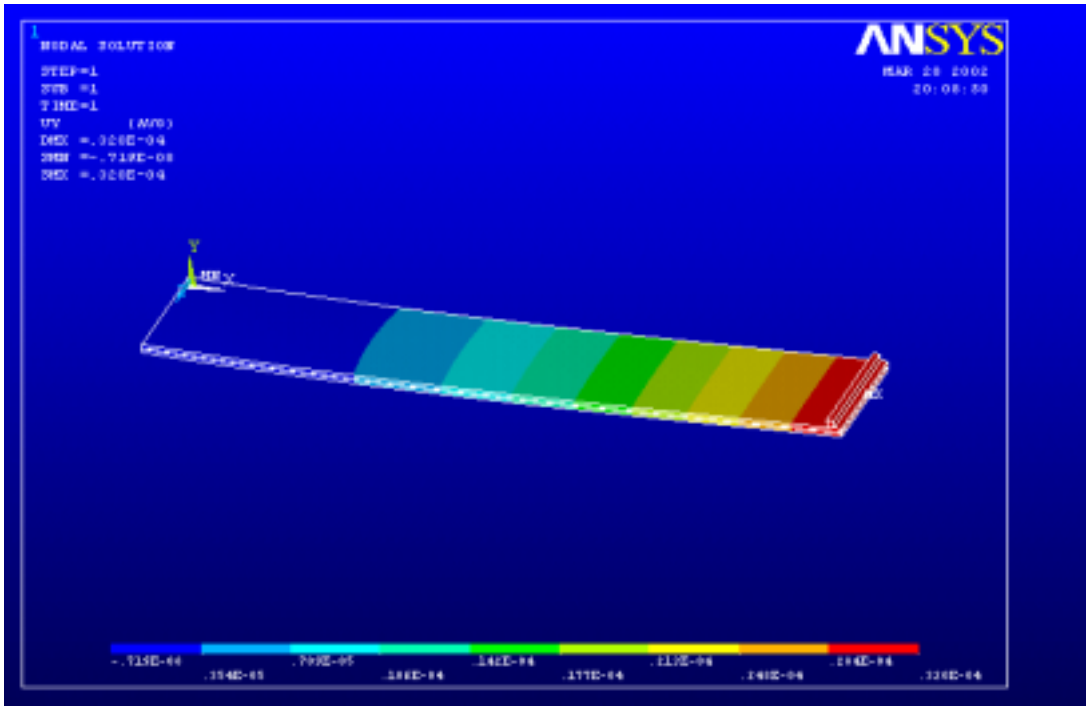


Figure 19 Blocked Force Calculation Using ANSYS

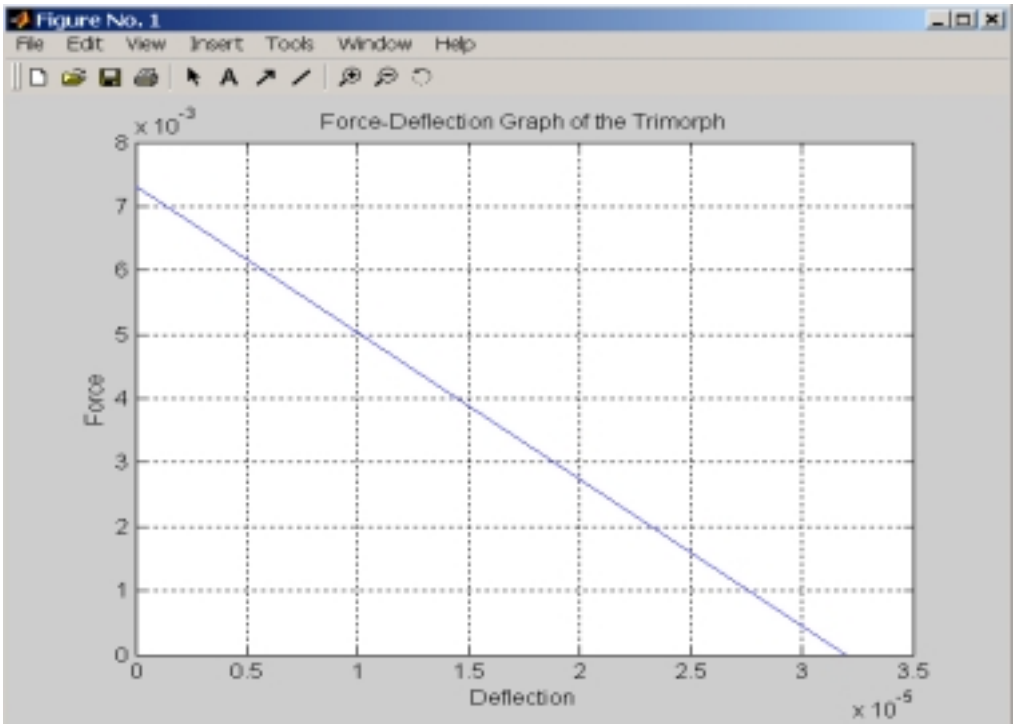


Figure 20 Force-Deflection Diagram of the Actuator

The total force on the bender was calculated to be $3\times10^{-5}$ N. That force is marked on the force deflection graph and corresponding deflection value is taken as the deflection of the actuator when the fluidic forces are taken into account. From Figure 21 the operating point of the piezo actuator under the influence of fluidic forces can be seen.

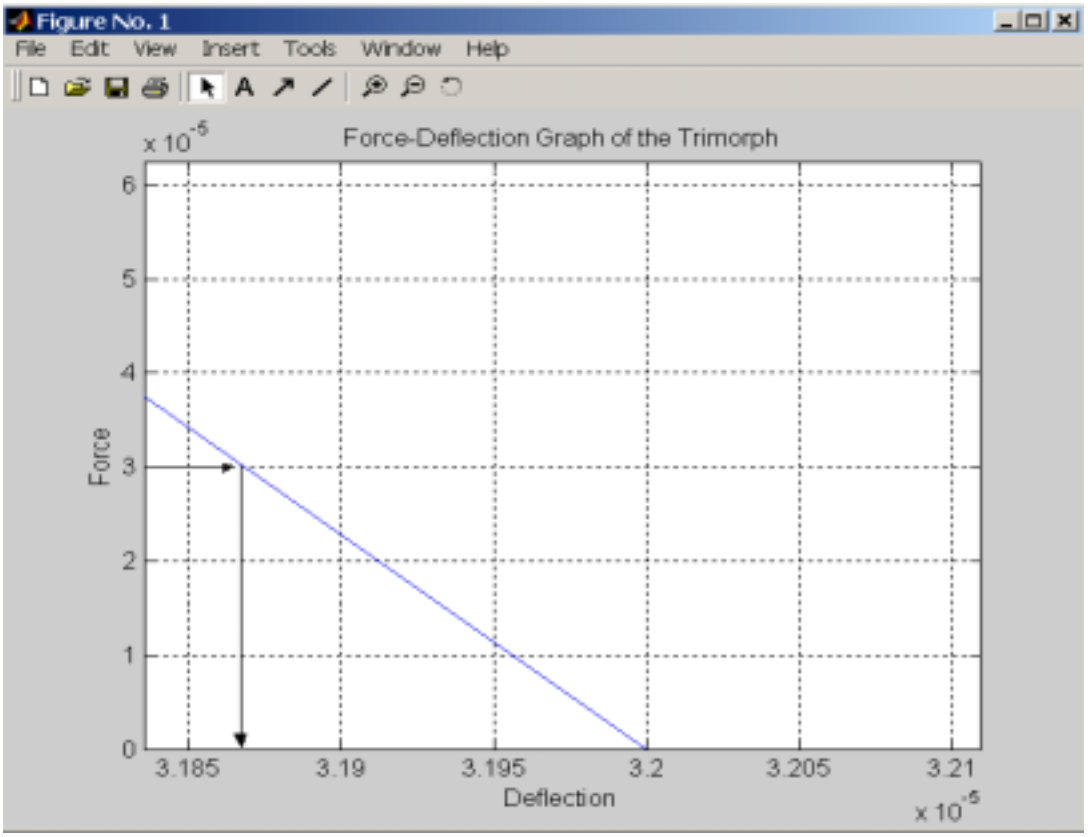


Figure 21 Close up of Force-Deflection Curve Considering Fluidic Forces

From this figure, it can be seen that the fluidic forces cause a loss of only 0.13 μm from the free deflection. From this result, it can be concluded that the valve can operate effectively under the maximum pressure difference and maximum velocity conditions. The fluid flow creates forces against the valve deflection but these forces are at a level that they can not make a

considerable difference in the maximum bender deflection. The next and final step to find the deflection and stress distribution of the valve for the operating voltage is the thermal analysis.

### 4.4.3 Thermal Analysis

As mentioned in the physical design part, bending resulting from the change in temperature is avoided by using a trimorph actuator. But temperature change also leads to longitudinal elongation in the actuator. This elongation causes changes in the deflection and stress distribution over the actuator. It is also critical to estimate the location of the gate on the middle wafer. To evaluate the thermal effects, the number of degrees of freedom is increased and thermal material properties are added to current ANSYS model. A temperature change of 80°C is used for the model. A voltage of 5-Volts is applied to the actuator. During the thermal analysis, fluidic forces are also placed on the tip of the actuator to obtain the real actuation characteristics. With all the forces applied, deflection in *x* and *y* directions, stress distribution on the bender are obtained. Table 9 summarizes the forces, voltage and thermal loads on the actuator.

Table 9 Summary of the Loads on the Actuator

| **Load Type** | **Explanation** |
|---|---|
| Electrical | 10 Volts voltage |
| Fluidic | 30 μN vertical force on the gate resulting from drag and pressure |
| Thermal | 80°C temperature difference applied to the both sides of the actuator |

Thermal properties of the brass and piezo layers are tabulated in Table 10. Thermal conductivity of the lead zirconate titanate PZT-5H is estimated by dividing Aluminum's conductivity by 200. (Piezo Systems, Inc.)

Table 10 Thermal Properties of Brass and PZT 5H

| Thermal Property | Brass | PZT 5H |
|---|---|---|
| Thermal Expansion Coefficient | $19\times10^{-6}$ 1/°C | $4\times10^{-6}$ 1/°C |
| Thermal Conductivity | 65 | 1.75 |

Figure 22 shows the elongation of the actuator. It can be seen that the bender elongates 6 μm, which means a minimum clearance of 10 μm should be kept between the gate and the gate guide to avoid the middle wafer to the gate at high temperatures.

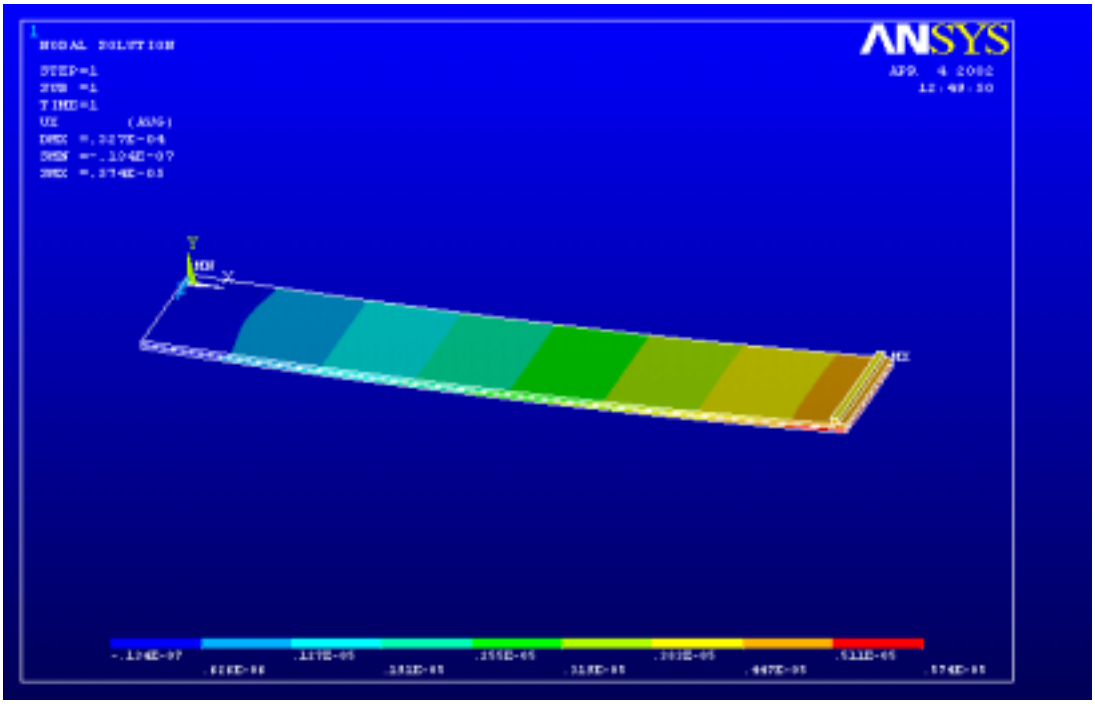


Figure 22 Longitudinal Displacement of the Actuator with 80°C Temperature Change

Another important parameter to check is the stress level under these conditions. Figure 23 shows the stress distribution over the actuator. The stress level on most of the parts is between 2 Mpa and 9 Mpa. A maximum stress of 63 MPa occurs on the brass shim near the cantilevered edge. The maximum stress on the piezo layers is calculated to be around 40 Mpa, which occurs on the cantilevered end and around the gate. Since the strength values for piezo and brass are 63 Mpa and 270 Mpa, microvalve operates safely under maximum temperature difference. These maximum stresses occur at 20°C since the actuator is cured at the operating temperature, 100°C. So, at the operating temperature, the stresses will be much lower.

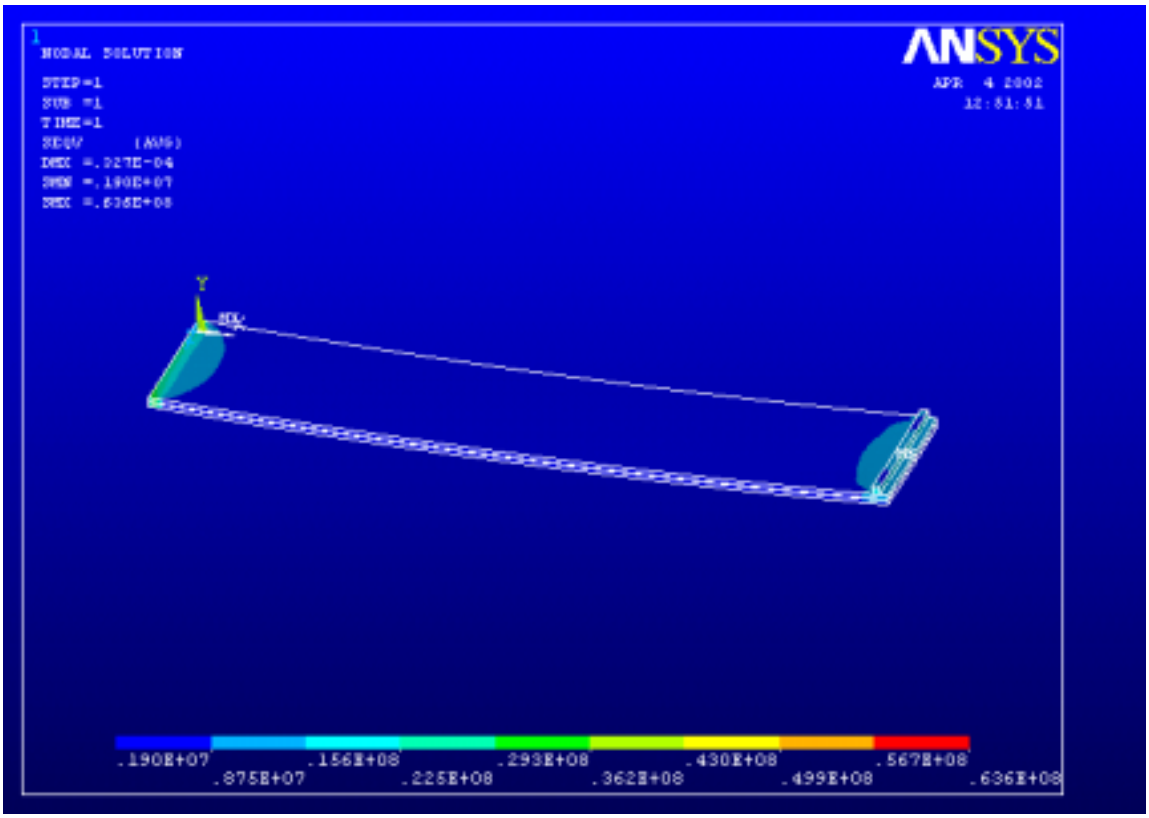


Figure 23 Stress Distribution with 80°C Temperature Change under 5V Excitation

Table 11 summarizes the final geometry, operating conditions and results such as maximum deflection, maximum stress values over the actuator. It also gives the failure strengths for actuator materials for a quick comparison with maximum stresses on them.

Table 11 Summary of Design

| Property | Value |
|---|---|
| Actuator length | 20 mm |
| Actuator width | 4 mm |
| Actuator thickness | 290 μm |
| Operating Voltage | 5 V |
| Temperature Difference | 80° C |
| Maximum Pressure Drop | 1 Psi |
| Maximum deflection | 32 μm |
| Maximum Elongation | 6 μm |
| Maximum Stress on Brass Shim (20ºC) | 63 Mpa |
| Operating Stress on Brass Shim (100ºC) | ≤ 3.2 Mpa |
| Brass Failure Stregth | 270 Mpa |
| Maximum Stress on Piezo Layers (20ºC) | 40 Mpa |
| Operating Stress on Piezo Layers (100ºC) | ≤ 3.2 Mpa |
| Piezo Failure Stregth | 63 Mpa |

# 5.0 FABRICATION

## 5.1 Micro Fabrication Methods

Fabrication basically involves two steps, material selection and construction. The silicon is the most widely used material in micro systems fabrication. Its good mechanical properties together with being one of very few materials that can be economically manufactured in single crystal substrates, make it the most suitable for many cases. Different compounds of silicon such as silicon oxide, silicon carbide and silicon nitride are also widely used in micro fabrication industry. The other common materials are thin metal films, polymers, glass and quartz substrates, piezoelectric ceramics and diamond.

The methods used in the fabrication of micro devices are different from the conventional methods. They are largely borrowed from the integrated circuit industry. Micro fabrication methods have limited capability so it is not possible to fabricate every shape in micro scale. The together with the other concerns, capabilities of the micro fabrication methods should be taken into account in the design stage.

Basic micromachining processes are deposition, patterning and etching. These processes can be grouped as bulk machining or subtractive micromachining and surface micromachining or additive micromachining. There are many different methods for each of these processes.

Deposition creates uniform thin layers. Epitaxy, oxidation, sputtering, evaporation, chemical vapor deposition, spin-on method, sol-gel process are common deposition methods. Each method has a different growth rate and different applications require different deposition methods to use. For example epitaxy is a common method to grow a crystalline silicon layer over a silicon wafer whereas sputtering is good for deposition of thin metals at low temperatures.

Patterning, also called as lithography, is a photographic process for printing images onto a layer of photosensitive polymer that is subsequently used as a mask against etching. Lithography has three steps; application of photoresist, optical exposure to print an image and immersion in an aqueous developer solution. If the photoresist is positive, exposed areas dissolve in the developer solution and if it is negative, exposed areas remain and unexposed areas dissolve. Contact, proximity and projection are the three methods for optical exposure. Resolution of these processes varies from 0.5 μm to 5 μm. Projection has the best resolution and proximity has the worst.

Etching is selectively removing material from a wafer. There are two types of etching which are isotropic and anisotropic. Anisotropic processes can further be grouped as wet and dry anisotropic etching. There are also electrochemical and plasma phase etching in some cases named as reactive ion etching (RIE) or deep reactive ion etching (DRIE). RIE and DRIE methods are used to create high aspect ratio channels. Isotropic etchants etch in all directions uniformly and create rounded cross sections whereas anisotropic etchants etch in one direction preferably over others and result in flat cross sections. HNA, also known as the poly-etch, is the most common isotropic etchant. It is a mixture of hydrofluoric (HF), nitric ($HNO_3$) and acetic

($CH_3COOH$) acids. NaOH, KOH and EDP (Ethylenediamine pyrochatechol) are well known anisotropic etchants. Figure 24 illustrates the resulting cross sections of isotropic and anisotropic etching processes.

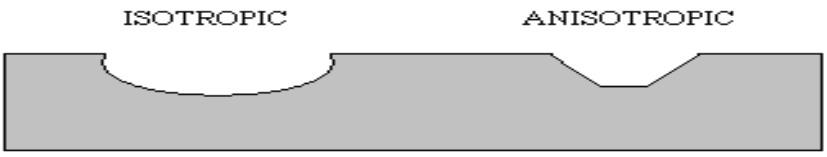


Figure 24 Resulting Cross Sections from Anisotropic and Isotropic Etching

Other main processes in micro fabrication can be listed as bonding, grinding, polishing, wiring and packaging. Bonding is the process of joining two parts together. Anodic and silicon fusion bonding methods are widely used bonding methods. Anodic bonding is used to bond a silicon wafer and a sodium-containing glass substrate. This bonding is performed at a temperature between 200° and 500°. Silicon fusion bonding, on the other hand, is used to bond two silicon substrates. This bonding takes place at a temperature between 300° and 800°. Silicon fusion bonding leaves almost no thermal stress on the resulting parts and after the process, the bond has the same mechanical strength as silicon. Another option is using adhesives for bonding. Epoxy adhesives provide safe operation for a good range of temperature and stress conditions. For the microvalve, a thin epoxy-phenolic, M-Bond 610 from Measurement Groups Inc., is selected for bonding to avoid high temperature and pressure forces that appear in the other methods.

Grinding and polishing are applied to achieve thickness reduction on a wafer. Grinding thin wafers is difficult since thin wafers are very fragile. Chemo-mechanical polishing combines mechanical polishing with chemical etching and it creates very smooth surfaces. Since we are using 127 μm standard piezo elements, no grinding or polishing is needed.

The purpose of wiring is to establish electrical connections within the micro device. There are mainly two types of wires, aluminum and gold, used in micro fabrication. Wire selection is done according to system requirements such as required length, current and system voltage.

## 5.2 Detailed Fabrication Plan for the Microvalve

### 5.2.1 Material Selection

Operation temperature and pressure, micro-fabrication compatability and resistance to hydrogen are the main concerns for material selections. Among these requirements hydrogen resistance seems to be the most important one since the operation temperature and pressure are within acceptable limits for most of the micro fabrication materials.

Hydrogen damage, also called hydrogen embrittlement, is a form of environmentally assisted failure that results most often from the combined action of hydrogen and residual or applied tensile stress. Hydrogen embrittlement affects many metals and alloys and it can occur in many ways, such as cracking, blistering, hydride formation and loss in tensile ductility. It is often

classified into three types; internal reversible embrittlement, hydrogen environment embrittlement and hydrogen reaction embrittlement. High temperature and pressure increase hydrogen damage on materials. Stress on metals can also increase the hydrogen diffusion into the material, which causes crack initiation. This crack initiation occurs at lower stress levels for ductile metals.

Considering all the parameters above, silicon, PZT-5H type lead zirconate titanate, brass and 440 stainless steel are selected for microvalve fabrication. Silicon is a single crystal material, which has a very low hydrogen diffusion rate so that no crack initiation occurs. It is fully compatible for distributions of high purity gases such as hydrogen. (Maluf,N., 2000) Brass is a copper alloy. Copper alloys are widely used in many environment and applications because of their excellent corrosion resistance together with the other desirable properties such as superior electrical and thermal conductivity, ease of fabricating and joining and wide range of attainable mechanical properties. Copper and its alloys are not susceptible to attack by hydrogen unless they contain copper oxide. (ASM Metals Handbook, Vol. 13) When oxygen-containing copper is heated, hydrogen diffuses into the metal and reacts with the oxide to form water, which decreases the ductility of the metal. Since brass does not contain copper oxide elements it is safe to use in a hydrogen environment. Stainless steel 440 is one of the steel types that is not susceptible to hydrogen attack. (ISA Handbook, 2$^{nd}$ Edition)

PZT-5H type lead zirconate titanate piezo ceramic element is used as the actuator material. This piezo ceramic material is not considered susceptible to any type of hydrogen embrittlement especially at temperatures around 100°C, which is the average operating

temperature for PEM fuel cells. Nickel as a material has already been used in solid oxide fuel cells so the electrodes on the piezo layers are proven to be safe in hydrogen environment. (Fuel Cell Handbook 4th edition, DOE)

### 5.2.2 Fabrication Plan

As mentioned above, the microvalve has four parts; three wafers and the actuator. The actuator is a 22.5 mm trimorph piezoelectric bender. Piezoelectric sheets are of type PSI-5H4E lead zirconate titanate purchased from Piezo Systems Inc., Camridge, MA. They are originally 7.24 mm wide, 7.24 mm long and 127 μm thick. Piezo plates are first diced to obtain 22.5 × 20 mm single plates. The 25 μm thick brass is purchased and 22.5 × 20 mm layers are cut. Piezoelectric plates, brass layer and the valve gate are glued together using a thin, low viscosity epoxy-phenolic adhesive (M-Bond 610 Measurement Group Inc.) and cured at an elevated temperature for better cross-linking. With nominal 5 μm thick glue layers, 127 μm thick piezo layers and 25 μm thick brass layer, the total thickness of the actuator is 290 μm. A portion (0.50 mm) of the bender is left outside the valve for the ease of electrical connection and wiring. Piezoelectric plates already have their electrodes on one side and the brass layer in the middle creates the second electrode for both of them.

Among different etching techniques, DRIE seems to be the best for wafer production since vertical edges are needed in most places such as actuator bed and flow channels. DRIE also eliminates the need for further calculations for the alignment of the gate and gate guide, which would be a problem if chemical wet etching was used. Conventional DRIE machines have etching rates between 1.4 to 4 μm/min depending on the aspect ratio of the trenches. Etch rate

increases with decreasing the aspect ratio. Since the microvalve has all wide trenches, the etch rate is expected to be high. But considering the extra wide trenches which will decrease the etch rate, this rate can be assumed to be 2.7μm/min. With this etch rate, the etch times are estimated to be around 15 minutes for the upper wafer, 90 minutes for the middle wafer and 145 minutes for the lower wafer. During etching, two points on all parts are marked for easy and accurate alignment during assembly. DRIE masks are given in Appendix C.

After the wafers are produced, the valve is assembled in the following order. First the actuator is glued on the lower wafer and cured at an elevated temperature. Then, middle part is glued on the lower wafer. Alignment of the gate and gate guide is very critical for the valve operation. Finally, the upper wafer is glued on top of the middle wafer. After the assembly, two valves are stacked together using the thin epoxy. Before placing into the hydrogen channel entrance, the electrical connections are completed. The microvalves can be sealed with teflon after the installation.

# 6.0 CONCLUSION AND FUTURE WORK

In this thesis, a novel piezoelectrically actuated microvalve for flow control in fuel cells was presented. Electro-mechanical, fluidic and thermal analyses were completed and the results presented.

The microvalve has overall dimensions of 22.5 × 20 × 1 mm. It has a piezoelectric trimorph actuator with dimensions of 22500 × 4000 × 290 microns. 25 μm brass shim was sandwiched between two 127 μm PZT-5H type lead zirconate titanate piezo layers. Brass was selected because of its resistance to hydrogen damage. 127 μm piezo layers are purchased from Piezo Systems Inc., Cambridge, MA. Before selecting the dimensions for the final design, a parametric study was performed to determine the effects of the operating voltage and bender dimensions on the maximum free deflection of the actuator. Results were tabulated and presented in the electro-mechanical analysis section. The final design geometry was chosen to be 4 mm wide, 30 μm high with the operating voltage of 5 Volts. The free deflection of the bender under 5 Volts operating voltage was calculated to be 32 μm. Fluidic analyses were the next step in design process. First, flow parameters such as Reynolds number, Mach number and Knudsen number were calculated to determine the appropriate flow model for the hydrogen. Then, flow rate, flow velocity, drag force, pressure force calculations were performed. Equivalent vertical forces of drag and pressure forces were calculated to be 16 and 14 μN respectively. Blocked force of the trimorph was calculated and force-deflection diagram of the trimorph was drawn. Using the equivalent forces calculated before, the deflection of the bender under the influence of fluidic forces was found to be 31.87 μm. The final step to determine the real operating conditions for

the actuator was completing the thermal analysis. A temperature difference of 80°C was used in the thermal analysis. The deflection, elongation and stress distribution over the actuator were determined with the ANSYS model. The maximum deflection of the bender under the influence of all forces was calculated to be 32 μm. Thermal forces caused an increase in the deflection which compensated the 0.13 μm loss from the fluidic forces. The same forces caused an elongation of 6 μm. The maximum stress on the brass shim was appeared to be 63 MPa, whereas the maximum stress on the piezo layers was 40 MPa. A factor of safety of 1.5 for piezo layers and 4.5 for brass shim were obtained since the strength values for brass and piezo are 63 and 270 MPa respectively. These maximum stresses occur at room temperature and much lower stresses occur at operating temperature.

A detailed fabrication plan was prepared for the microvalve. Among different etching techniques, DRIE was chosen since vertical trench walls are required. A low viscosity, thin epoxy-phenolic, M-Bond 610, Measurement Groups Inc., was chosen for bonding the actuator parts as well as the wafers to each other for good strain transfer. All parts will be cured at elevated temperatures for improved cross linking. After the fabrication was complete, two microvalves were stacked together using the same glue. The microvalve stack will then be tested and ultimately placed at the entrance of the hydrogen channels. Silicone or teflon will be used to seal the gaps.

The future work includes the detailed fluidic analysis and modification of the microvalve for solid oxide fuel cells. Pressure drop and flow profiles for all positions of the gate will be modeled in ANSYS. Modification for solid oxide fuel cells is a more complicated task since the

operating conditions of these fuel cells are much different than PEM fuel cells. The main problem is the temperature, which averages around 800-1000°C in the solid oxide fuel cells. A temperature difference of 80°C created a maximum stress of 63 MPa on the actuator. The current microvalve design would fail under a temperature difference of 1000°C with the current material selection. The elongation of the actuator will also be very high and it will bring more clearance requirement for the design and increase the leakage rate. Also the piezo layers will depole at such high temperatures. For the analyses, a metal of higher strength and lower thermal expansion coefficient and a bond that will survive such thermal expansions can be a good selection to start with.

# APPENDICES

## Appendix A

## MATLAB Codes for Fluidic Analsis

```
mu = 8.82e-6;                                   % kg/m/s, coeff of viscosity
rho = .0704;                                    % kg/m^3, density
eta = 1.05e-4;                                  % m^2/s,  kinematic viscosity, eta = mu/rho
k = 1294;                                       % m/s, sound speed of H2, White, p. 517
Cpc = R_h2*(3.057 + 2.677e-3*TT -5.810e-6*TT^2 + 5.521e-9*TT^3 -1.812e-12*TT^4)
Cvc = Cpc - R_h2
gamma = Cpc/Cvc                                 % constant with temp according to White, p.
513.
TT = 273+100
R_h2 = R/2;                                     % gas constant for hydrogen
c = sqrt(gamma*R_h2*TT)                         % (m/s) sound speed of H2 at 100 deg. C


g = 9.81;                                       % m/s, acceleration due to gravity.
L = 22.2e-3;                                    %(m), total length of flow channel
w = 4e-3                                        %(m) Width of the channel
h = 30e-6                                       %(m) Height of the channel
n = 2;                                          % number of valves
```

```
Q_l = 0.441;                    %Total Flow rate in SLPM
Q = (Q_l/1000)/60./n;           % Flow rate in m^3/s for each valve in stack
mdot1 = Q*rho                   %mass flow rate
A = w*h;                        % m^2, Area of the flow

v = Q/A;                        %Velocity in m/s
Mach = v/k                      %Mach number
R  = 8314;                      % m^2/K/s^2, ideal gas constant
T  = 373;                       % degrees Kelvin, temperature
Cd = 0.9;                       % assume nearly perfect, Coeff. of discharge
Re = rho * v * Dh / muc         % Reynolds number

% Worst case drag force

Fd  = 1/2 *Cd*rho*(v*5)^2*w*h       % Drag force, assume velocity increases by
10x
M   = (185+145)*1e-6*Fd             % Moment cause by dynamic force
Feq = M/20e-3                       % Equivalent vertical force at tip

% Pressure differential force.

Fp   = 1 * 6895 * 30e-6 * 4e-3      %Pressure force
```

```
Mp   = (185+145)*1e-6*Fp                % Moment cause by dynamic force

Feqp = Mp/20e-3                         % Equivalent vertical force at tip


% Knudsen number, p.14 Microflows by Karniadakis

Kn = sqrt(pi*gamma/2)*Mach/Re           % Knudsen Number (< 0.01), continuum regime
```

# Appendix B

## Microvalve Drawings*

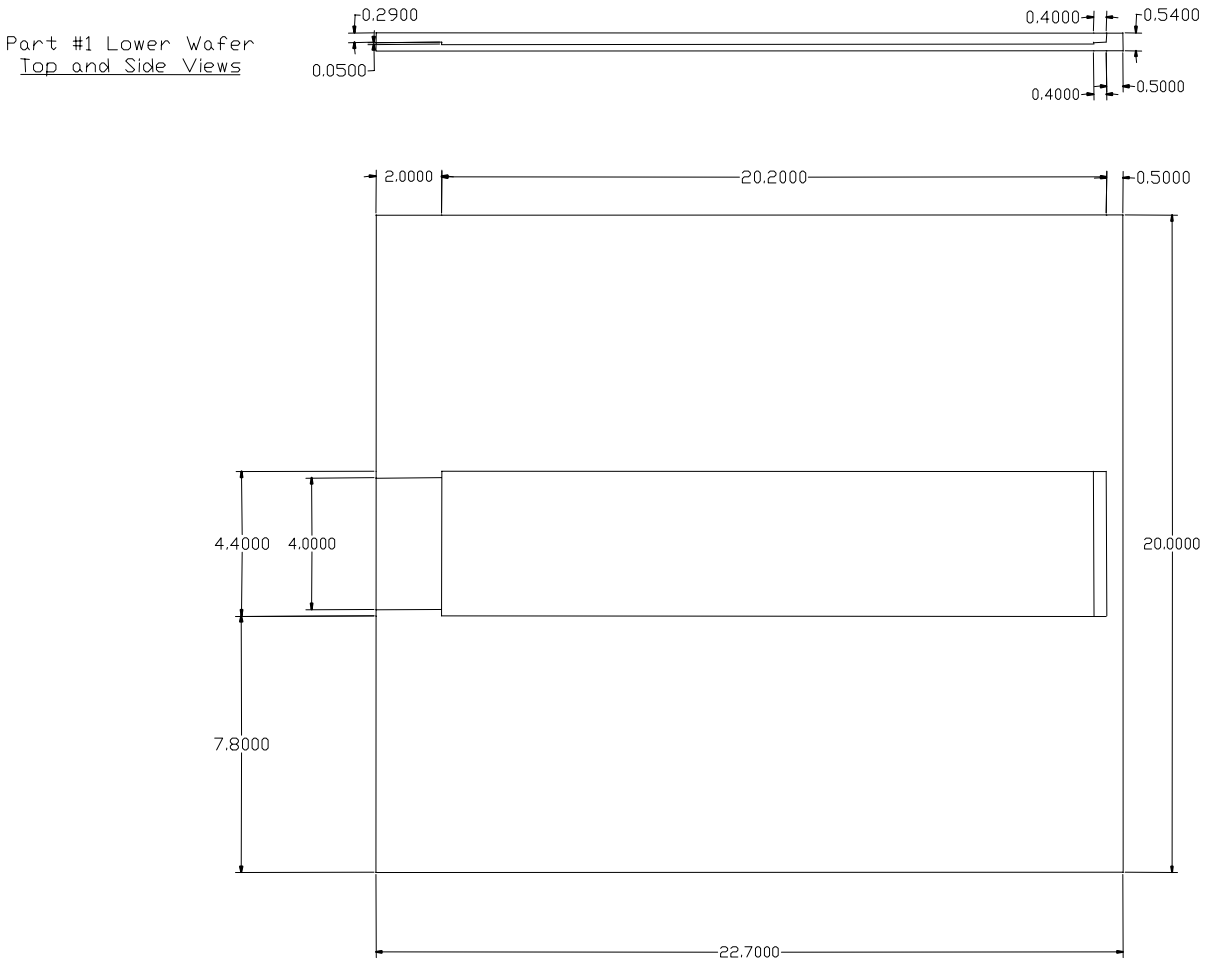


* All dimensions in the drawings are in milimeters

Part #2 Middle Wafer
Bottom and Side Views

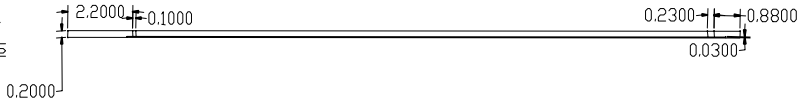


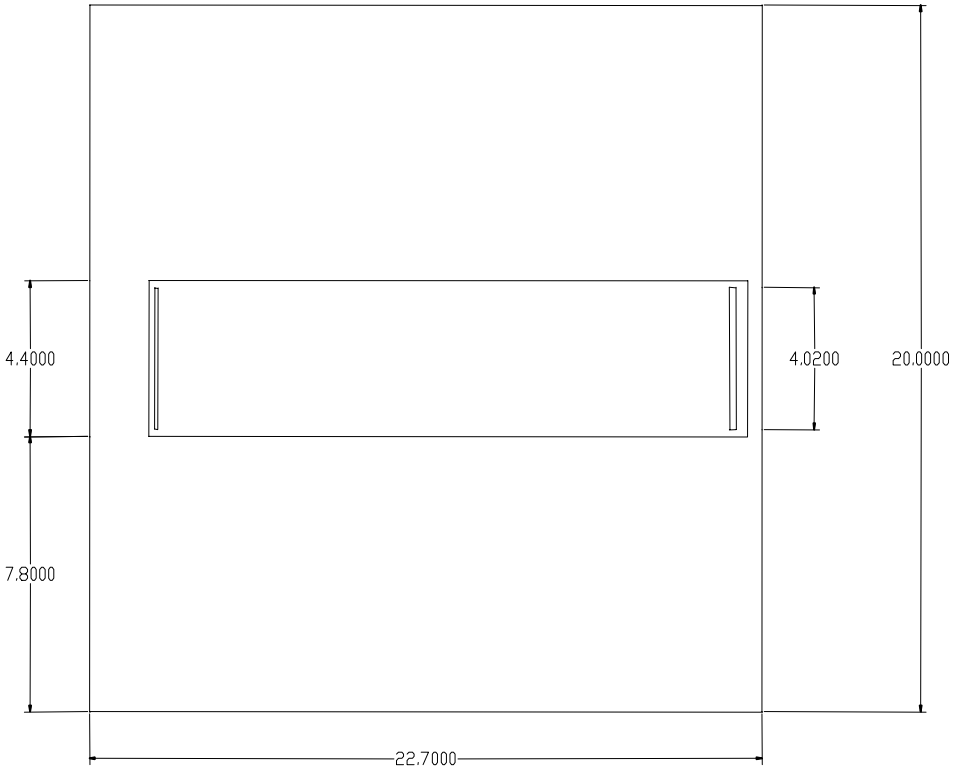

Part #3 Upper Wafer
Bottom and Side Views


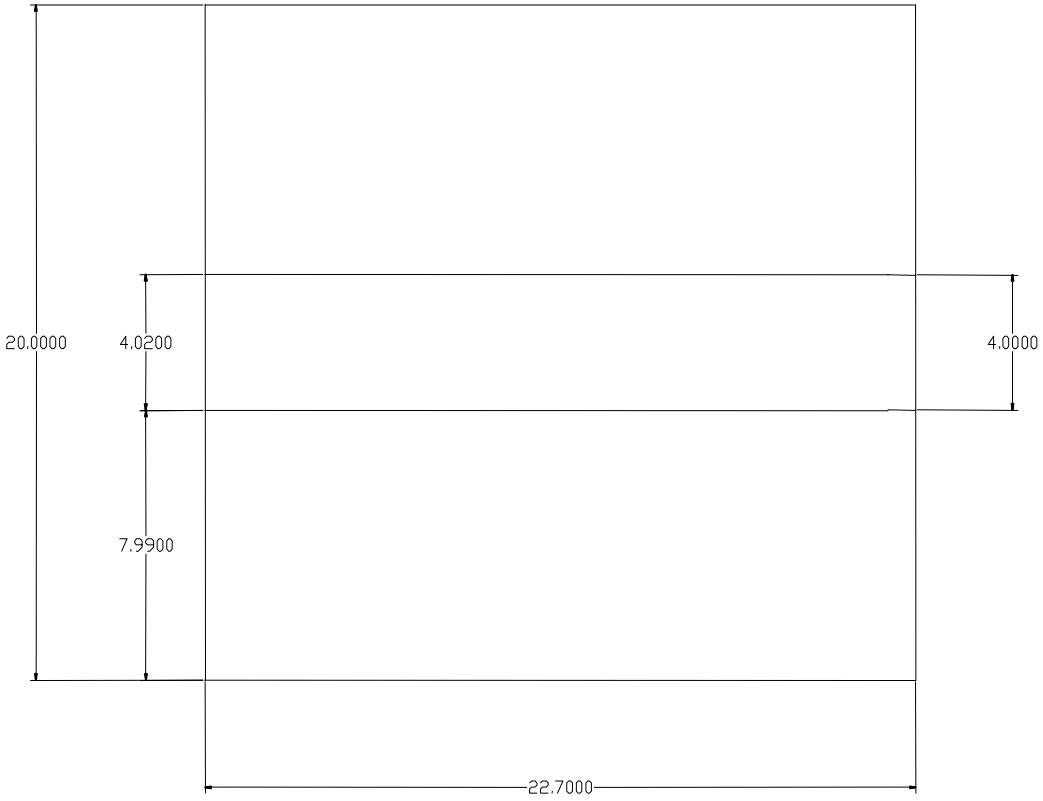

MICROVALVE ASSEMBLY
CROSS SECTIONAL VIEW

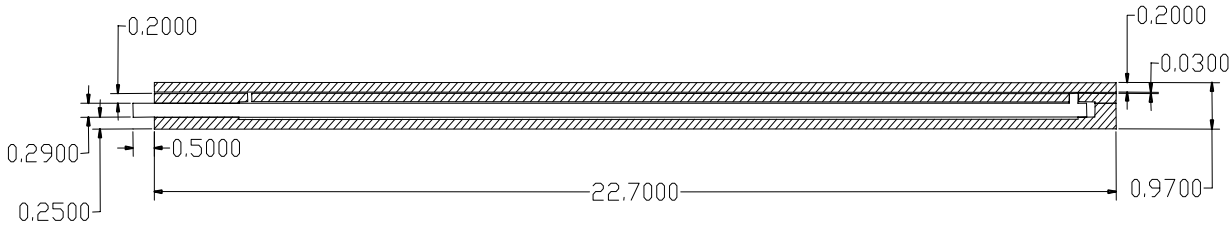


Actuator Assembly

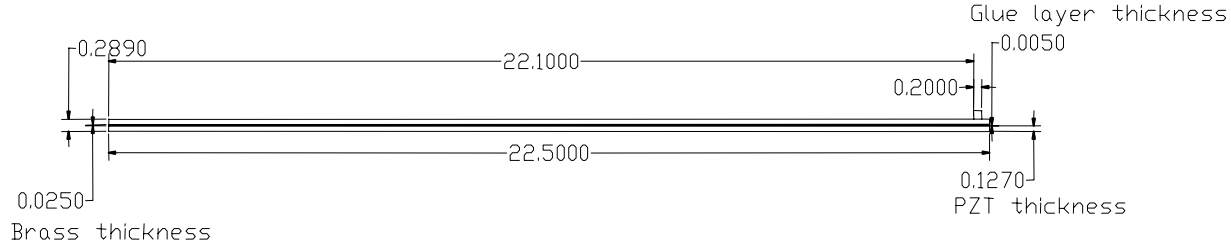

# Appendix C

## DRIE Mask Drawings

DRIE Mask #1
Lower Wafer
290 microns actuator bed etch

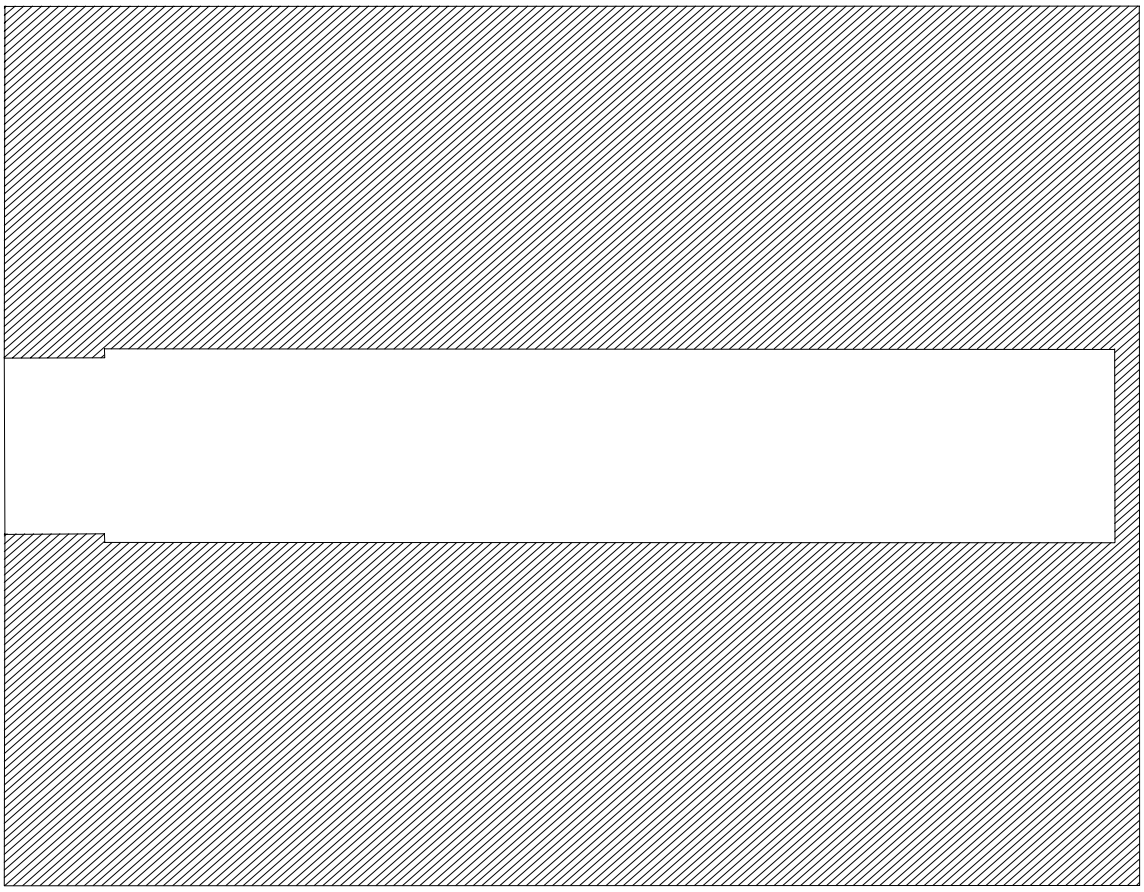

DRIE Mask #2
Lower Wafer
50 microns hole etch under the actuator

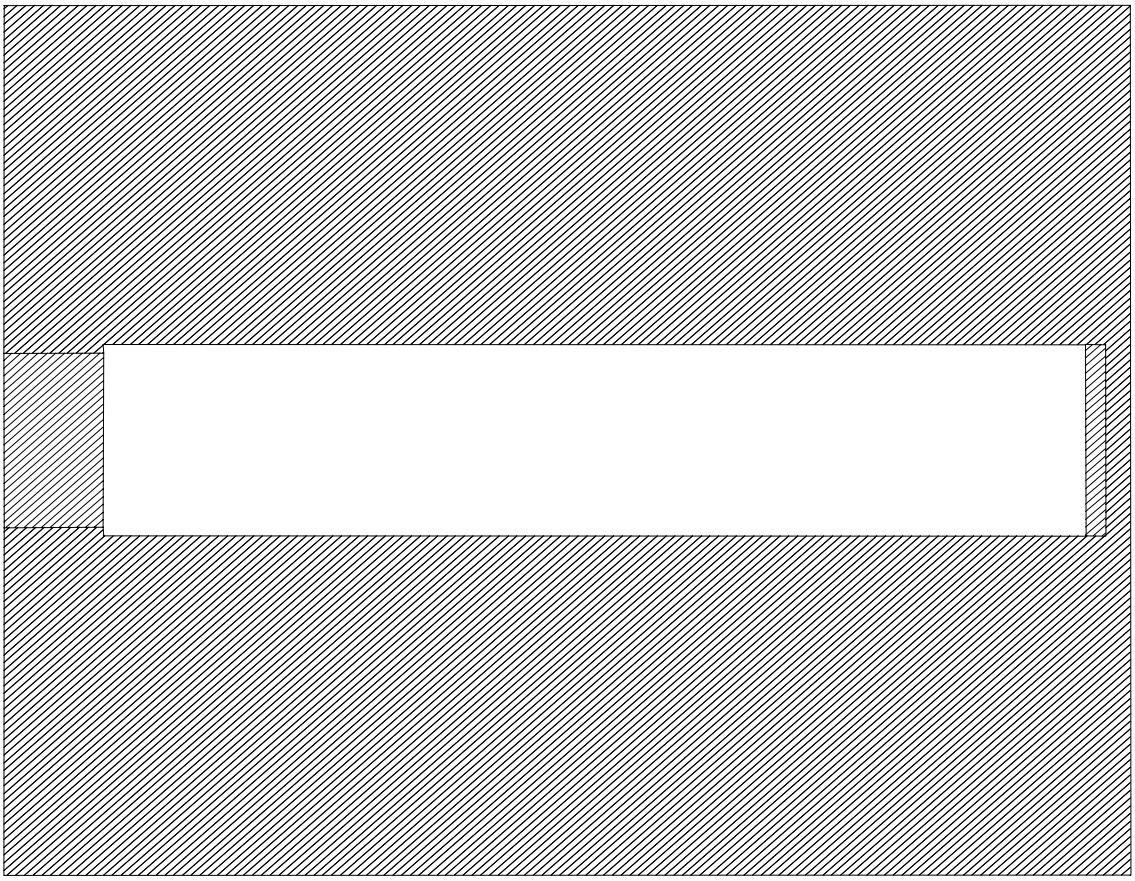

DRIE Mask #3
Middle Wafer
30 microns actuator hole etchle etch

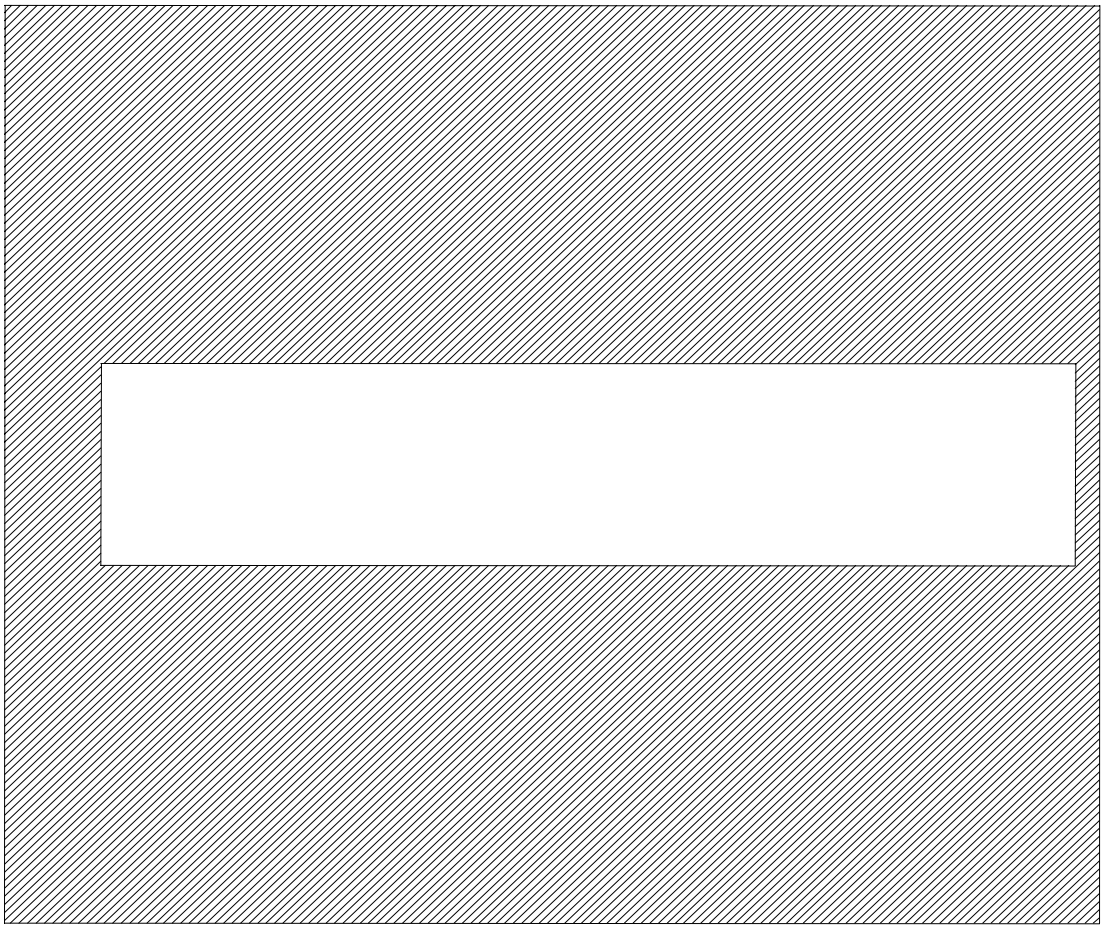

DRIE Mask #4
Middle Wafer
170 microns gate guide and pressure hole etch

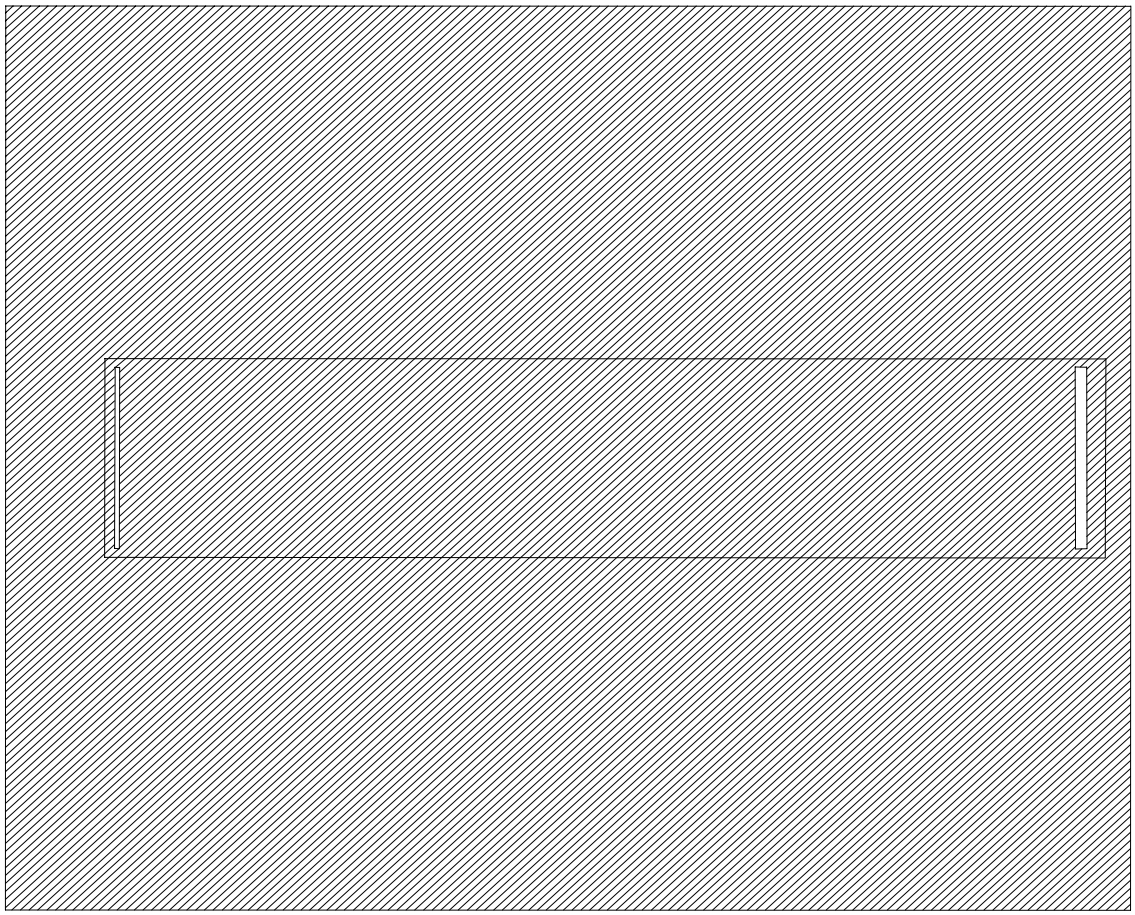

DRIE Mask #5
Upper Wafer
30 microns flow channel etch

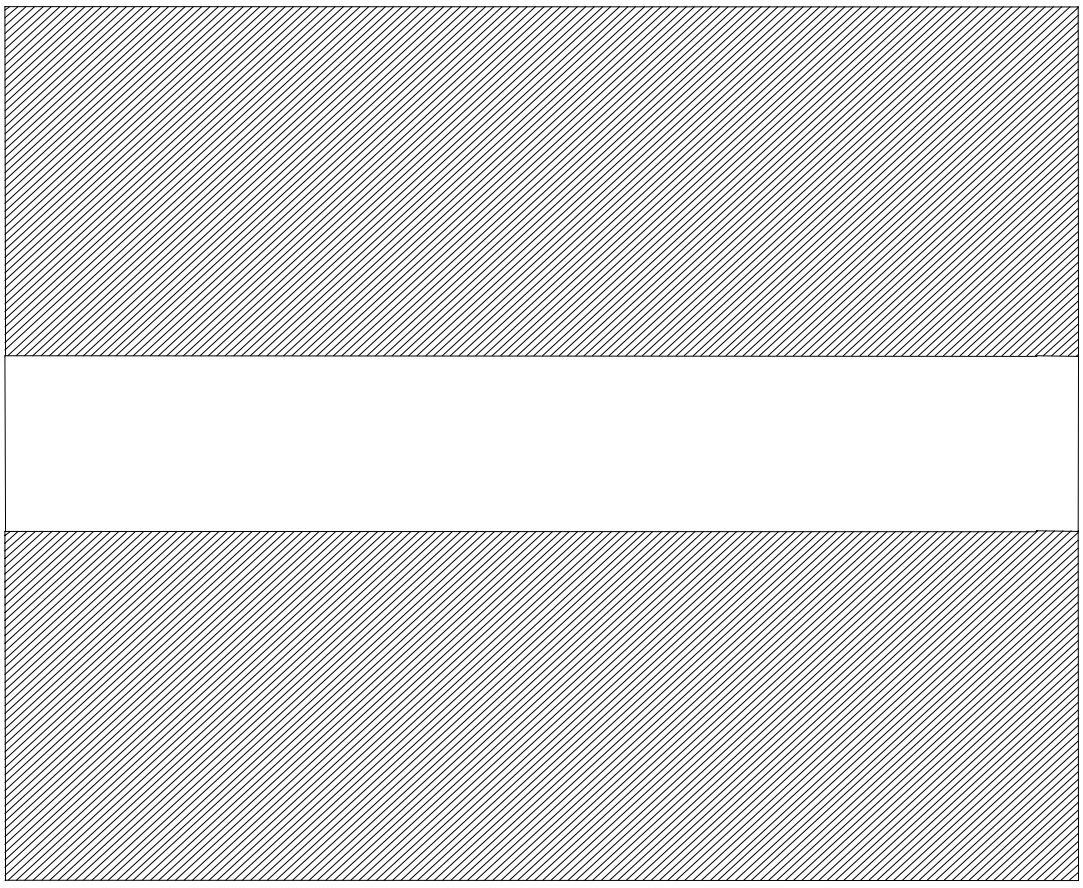

# BIBLIOGRAPHY

## BIBLIOGRAPHY


1. Askeland, D. R., "The Science and Engineering of Materials", (Boston: PWS Publishing, 1994)

2. Capanu, M. Boyd, J. G. IV, Hesketh, P. J., "Design, Fabrication, and Testing of a Bistable Electromagnetically Actuated Microvalve", Journal of Microelectromechanical Systems, Vol. 9, No. 2, June 2000

3. Chakraborty, I., Tang, W. C., Bame,. D., Tang, T. K., "Normally Closed Piezoelectrically Actuated Microvalve", NASA Tech Brief Vol. 25, No. 1, 2001

4. Chou, T. A., Najafi, K., "3D MEMS Fabrication Using Low-Temperature Wafer Bonding with Benzocyclobutene (BCB)"

5. Craig, B., "Hydrogen Damage", ASM Metals Handbook, Vol. 13

6. Hatchison, J. ,W., ISA Handbook of Control Valves, 2nd Edition, Instrument Society of America, PA, 1976

7. Henning, A. K., "Microfluidic MEMS", IEEE 1998

8. Hidenori I., Furmihito A., and Toshio F., "Micro Mechatronics and Micro Actuators", IEEE/ASME Transactions on Mechatronics, Vol.1, No.1, March 1996

9. Hirschenhofer, J. H., Stauffer, D. B., Engleman, R. R., Klett, M. G., Fuel Cell Handbook, Fourth Edition, U.S. Department Of Energy, Nov. 1998

10. Hosokawa K., Maeda R., "A Pneumatically-Actuated Three-way Microvalve Fabricated with Polydimethylsiloxane Using the Membrane Transfer Technique", Journal of Micromechanics and Microengineering, 2000

11. Ilzhofer, A., Ritter, B., Tsakmakis, C., "Development of Passive Microvalves by Finite Element Method", Journal of Micromechanics and Microengineering, 1995

12. Jensen, S. O., Gravesen, P., "Flow Characteristics of a Micromachined Diaphragm Valve Designed for Liquid Flows Above 1ml/min", Journal of Micromechanics and Microengineering, 1993

13. Jerman, H., "Electrically-Activated, Normally-Closed Diaphragm Valves", Journal of Micromechanics and Microengineering, 1994

14. Joswig, J. "Active Micromechanic Valve", Journal of Micromechanics and Microengineering, 1992

15. Karniadakis, G. E., Beskok, A., "Micro Flows Fundamentals and Simulation", (New York: Springer-Verlag, 2002)

16. Koch, M., Evans, A. G. R., Brunnschweiler, A., "Coupled FEM Simulation for Characterizaation of Fluid Flow within a Micromachined Cantilever Valve"

17. Koch, M., Evans, A.G. R., Brunnschweiler, A., "Characterization of micromachined cantilever valves", Journal of Micromechanics and Microengineering, 2001

18. Kohl, M., Dittmann, D., Quandt, E., Winzek, B., Miyazaki, S., Allen, D. M., "Shape memory Microvalves Based On Thin Films on Rolled Sheets", Journal of Materials and Science Engineering, 1999

19. Kohl, M., Skrobanek, K. D., Miyazaki, S., "Development of Stress-optimised Shape Memory Microvalves", Journal of Sensors and Actuators, 1999

20. Kovacs, G. T. A., "Micromachined Transducers Sourcebook", (NewYork: McGraw-Hill, 1998)

21. Maluf, N., "An Introduction to Microelectromechanical Systems Engineering", ( NewYork, London: Artec House, 2000)

22. Michel, F., Ehrfeld, W., "Mechatronic Micro Devices", International Symposium on Micromechatronics and Human Science, IEEE, 1999

23. Osterbroak, R. E., Berenschot, J. W., Schlautmann, S., Krijnen, G. J. M., Lammerink, T. S. J., Elwenspoek, M. C., Van Den Berg, A., "Designing, Simulation and Realization of In-plane Operating Microvalves Using New Etching Techniques", Journal of Micromechanics and Microengineering, 1999

24. Paul, B. K, Terhaar, T., "Comparison of two passive microvalve designs for microlamination architectures", Journal of Micromechanics and Microengineering, 2000

25. Polan N. W., "Corrosion of Copper and Copper Alloys", ASM Metals Handbook, Vol. 13

26. Raymond, L., "Evaluation of Hydrogen Embrittlement", ASM Metals Handbook, Vol. 13

27. Robertson, J. K., Wise K. D, "A low pressure micromachined flow modulator", Journal of Sensors and Actuators, 1998

28. Ruffieux, D., Dubois, M. A., Rooij, N. F., "An ALN Piezoelectric Microactuator Array", IEEE, 2000

29. Ruzzu, A., Bade, K., Fahrenberg, J., Maas, D., "Positioning System for Catheter Tips Based on Active Microvalve System", Journal of Micromechanics and Microengineering, 1998

30. Sadler, D.j., Kwang, W. O., Ahn, C. H., Bhansali, S., Henderson, H. T., "A New Magnetically Actuated Microvalve for Liquid and Gas Control Applications"

31. Shoji, S., "Fluid for Sensor Systems", 1998

32. Shoji, S., Van Der Schoot, B., Rooji, N., Esashi, M., "Smallest Dead Volume Microvalves for Integrated Chemical Analyzing Systems", IEEE, 1991

33. Sitti, M., Campolo, D., Yan, J., Fearing R. S., "Development of PZT-PT Based Unimorph Actuators for Micromechanical Flapping Mechanisms"

34. Vandelli, N., Wroblewski, D., Velonis, M., Bifano, T., "Development of a MEMS Microvalve Array for Fluid Flow Control", Journal of Micromechanics and Microengineering, 1998

35. Voldman, J., Gray, M. L., Schmidt, M. A., "An Integrated Liquid Mixer/Valve", Journal of Microelectromechanical Systems, Vol. 9, No. 3, Sept 2000

36. Wang, X., Zhou, Z., Ye, X., Yi, Y., Zhang, Z., "A PZT-driven Micropump", International Symposium on Micromechatronics and Human Science, IEEE, 1998

37. Yang, X, Grosjean, C.,Tai, Y, "Design, Fabrication, and Testing of Micromachined Silicone Rubber Membrane Valves", Journal of Micromechanical Systems, December 1999

38. Yang, X., Grosjean, C., Tai, Y., Ho, C., "A MEMS Thermopneumatic Silicone Membrane Valve"

39. Yobas, L., Carver, B. R., Lisy, F., Huff, M. A., "Elecrtrostatically Actuated MEMS Microvalve suitable for Pneumetically Refreshed Braille-Display System"

40. Yuen, P. K., Kricka, L. J., Wilding, P., "Semi-disposable Microvalves for Use with Microfabricated Devices or Microchips", Journal of Micromechanics and Microengineering, 2000